

APR 25 2006

REPORT DOCUMENTATION PAGE			Form Approved OMB No. 0704-0188	
Public reporting burden for this collection of information is estimated to average 1 hour per response, including the time for reviewing instructions, searching existing data sources, gathering and maintaining the data needed, and completing and reviewing the collection of information. Send comments regarding this burden estimate or any other aspect of this collection of information, including suggestions for reducing this burden, to Washington Headquarters Services, Directorate for Information Operations and Reports, 1215 Jefferson Davis Highway, Suite 1204, Arlington, VA 22202-4302, and to the Office of Management and Budget, Paperwork Reduction Project (0704-0188), Washington, DC 20503.				
1. AGENCY USE ONLY (Leave blank)	2. REPORT DATE 20.Apr.06	3. REPORT TYPE AND DATES COVERED THESIS		
4. TITLE AND SUBTITLE DYNAMIC RESPONSE OF SUPER-HEATED LIQUID DROPLETS IN STEADY SUPERSONIC AIRFLOW		5. FUNDING NUMBERS		
6. AUTHOR(S) 2D LT JORDAN NATHAN C				
7. PERFORMING ORGANIZATION NAME(S) AND ADDRESS(ES) UNIVERSITY OF WASHINGTON		8. PERFORMING ORGANIZATION REPORT NUMBER CI04-1768		
9. SPONSORING/MONITORING AGENCY NAME(S) AND ADDRESS(ES) THE DEPARTMENT OF THE AIR FORCE AFIT/CIA, BLDG 125 2950 P STREET WPAFB OH 45433		10. SPONSORING/MONITORING AGENCY REPORT NUMBER		
11. SUPPLEMENTARY NOTES				
12a. DISTRIBUTION AVAILABILITY STATEMENT Unlimited distribution In Accordance With AFI 35-205/AFIT Sup 1		12b. DISTRIBUTION CODE		
13. ABSTRACT (Maximum 200 words)				
DISTRIBUTION STATEMENT A Approved for Public Release Distribution Unlimited				
14. SUBJECT TERMS			15. NUMBER OF PAGES 96	
			16. PRICE CODE	
17. SECURITY CLASSIFICATION OF REPORT	18. SECURITY CLASSIFICATION OF THIS PAGE	19. SECURITY CLASSIFICATION OF ABSTRACT	20. LIMITATION OF ABSTRACT	

Dynamic Response of Superheated Liquid
Droplets in Steady Supersonic Airflow

Nathan C. Jordan

A thesis
submitted in partial fulfillment of the
requirements for the degree of

Master of Science in Aeronautics and Astronautics

University of Washington

2006

Program Authorized to Offer Degree:
Aeronautics and Astronautics

20060501304

ABSTRACT

Dynamic Response of Superheated Liquid Droplets in Steady Supersonic Airflow

Nathan C. Jordan

Chair of the Supervisory Committee:
Associate Professor James C. Hermanson
Department of Aeronautics and Astronautics

Individual 70 μ m diameter droplets of ethanol, 1-propanol, and hexanol were smoothly accelerated to supersonic conditions relative to the droplets in a convergent, free-expansion nozzle. The velocities of the droplets were measured, from which the acceleration of the droplets was determined in a supersonic airflow of known properties. Droplets were illuminated by a double-pulsed laser and imaged by an ICCD camera. Dividing the distance between the resulting two images of the drop by the known time step gave a velocity, at a given downstream distance. The measured results were compared to those of a dynamic droplet acceleration model based on a rigid sphere of the same diameter. The droplets achieved a peak Mach number relative to the surrounding air flow of approximately 3.5.

The three test fluids had similar physical characteristics except for vapor pressure, allowing for variation in the degree of superheat the droplets of

loss until they were finally completely disrupted.

Population histograms as a function of downstream distance confirm progressive disruption of the droplets downstream of the nozzle throat. The histograms also indicate that there is a small effect of the degree of superheat on the rate at which the populations of droplets decrease.

ABSTRACT

Dynamic Response of Superheated Liquid Droplets in Steady Supersonic Airflow

Nathan C. Jordan

Chair of the Supervisory Committee:
Associate Professor James C. Hermanson
Department of Aeronautics and Astronautics

Individual 70 μ m diameter droplets of ethanol, 1-propanol, and hexanol were smoothly accelerated to supersonic conditions relative to the droplets in a convergent, free-expansion nozzle. The velocities of the droplets were measured, from which the acceleration of the droplets was determined in a supersonic airflow of known properties. Droplets were illuminated by a double-pulsed laser and imaged by an ICCD camera. Dividing the distance between the resulting two images of the drop by the known time step gave a velocity, at a given downstream distance. The measured results were compared to those of a dynamic droplet acceleration model based on a rigid sphere of the same diameter. The droplets achieved a peak Mach number relative to the surrounding air flow of approximately 3.5.

The three test fluids had similar physical characteristics except for vapor pressure, allowing for variation in the degree of superheat the droplets of

loss until they were finally completely disrupted.

Population histograms as a function of downstream distance confirm progressive disruption of the droplets downstream of the nozzle throat. The histograms also indicate that there is a small effect of the degree of superheat on the rate at which the populations of droplets decrease.

Dynamic Response of Superheated Liquid Droplets in Steady Supersonic Airflow

Nathan C. Jordan

A thesis
submitted in partial fulfillment of the
requirements for the degree of

Master of Science in Aeronautics and Astronautics

University of Washington

2006

Program Authorized to Offer Degree:
Aeronautics and Astronautics

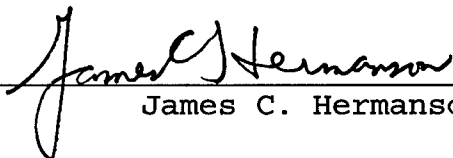
University of Washington
Graduate School

This is to certify that I have examined this copy of a
master's thesis by

Nathan C. Jordan

and have found that it is complete and satisfactory in all
respects, and that any and all revisions required by the
examining committee have been made.

Committee members:


James C. Hermanson


Mitsuru Kurosaka

Date: 16 Mar 06

In presenting this thesis in partial fulfillment of the requirements for a master's degree at the University of Washington, I agree that the Library shall make its copies freely available for inspection. I further agree that extensive copying of this thesis is allowable only for scholarly purposes, consistent with "fair use" as prescribed in the U.S. Copyright Law. Any other reproduction for any purposes or by any means shall not be allowed without my written permission.

Signature Nathan Jank

Date 16 Mar 2006

University of Washington

ABSTRACT

Dynamic Response of Superheated Liquid Droplets in Steady Supersonic Airflow

Nathan C. Jordan

Chair of the Supervisory Committee:
Associate Professor James C. Hermanson
Department of Aeronautics and Astronautics

Individual 70 μ m diameter droplets of ethanol, 1-propanol, and hexanol were smoothly accelerated to supersonic conditions relative to the droplets in a convergent, free-expansion nozzle. The velocities of the droplets were measured, from which the acceleration of the droplets was determined in a supersonic airflow of known properties. Droplets were illuminated by a double-pulsed laser and imaged by an ICCD camera. Dividing the distance between the resulting two images of the drop by the known time step gave a velocity, at a given downstream distance. The measured results were compared to those of a dynamic droplet acceleration model based on a rigid sphere of the same diameter. The droplets achieved a peak Mach number relative to the surrounding air flow of approximately 3.5.

The three test fluids had similar physical characteristics except for vapor pressure, allowing for variation in the degree of superheat the droplets of different liquids experienced. Superheating was achieved through the drop in static pressure in the free-expanding jet below the vapor pressure of the liquid at injection temperature. Based on the local static pressure in the supersonic air stream, the ethanol droplets achieved the maximum degree of superheat of all the droplets. The hexanol droplets did not experience superheating as the static pressure in the test section did not drop below the injection-temperature vapor pressure of hexanol. Immediately downstream of the bow shock wave the droplets of all three fuels were not superheated due to the static pressure rise across the shock. This suggests that the effects of superheating on droplet disruption and vaporization are greatest at the flanks of the droplets.

Comparison between the three fluids indicated that there was little difference in the acceleration or velocities achieved as a result of the varied degree of superheat. However, both the velocities and accelerations were considerably smaller than those predicted by the solid sphere model, indicating that the forces applied to liquid

drops in supersonic airflow are significantly impacted by the deformation and disruption of the liquid drops.

During their acceleration from the throat through the test section, the droplets disrupted and experienced mass loss until they were finally completely disrupted.

Population histograms as a function of downstream distance confirm progressive disruption of the droplets downstream of the nozzle throat. The histograms also indicate that there is a small effect of the degree of superheat on the rate at which the populations of droplets decrease.

TABLE OF CONTENTS

	Page
List of Figures	iii
List of Tables	vi
Glossary	vii
English	vii
Greek	vii
Subscript	viii
Preface	ix
Acknowledgements	x
Introduction	1
Experimental Setup	12
Wind Tunnel	12
Droplet Generation System	14
Supply System	15
Data Imaging System	18
Test Fluids	21
Data Processing	21
Computational Model	32
Model Structure	33
Computational Results	35
Breakup Mode Predictions	36
Experimental Results	39

Hexanol	40
1-Propanol	42
Ethanol	43
Droplet Population	45
Discussion	53
Summary and Conclusions	62
Future Work	70
Endnotes	72
References	76
Appendix A: A Sample Spreadsheet	80

LIST OF FIGURES

Figure Number	Page
1.1 Droplet Breakup Modes for Non-Volatile Droplets	10
1.2 Classification of Breakup Mode Based on Weber Number for Non-Volatile Droplets in Mach 3 Airflow	11
2.1 Test Section Mounted on PVC Elbow	24
2.2 Test Section Exterior	24
2.3 Test Section Interior	25
2.4 Centerline Mach Number, Normalized Static Temperature and Normalized Speed of Sound Determined From Pitot Probe Measurements	25
2.5 Centerline Air Velocity	26
2.6 Centerline Static Temperature	26
2.7 Centerline Static Pressure	27
2.8 Mach Disk Schlieren Photograph	27
2.9 DoD Droplet Generator	28
2.10 Physical Dimensions of DoD Device	28
2.11 Pressure/Vacuum Supply System	29
2.12 Diagram of Pressure/Vacuum Supply System	29
2.13 Sample Panasonic Camera Image Used Droplet Size and Spacing Verification	30
2.14 Triggering Sequence	30
3.1 Modeled Droplet Relative Velocity	37
3.2 Modeled Droplet Relative Mach Number	37

3.3 Modeled Droplet Weber Number	38
3.4 Modeled Droplet Reynolds Number	38
4.1 1-Propanol Droplet Multiple Exposure Image	47
4.2 Hexanol Droplet Multiple Exposure Image	47
4.3 Absolute Velocity of Hexanol Droplets Downstream of Throat Compared to Solid Sphere Model Predictions	48
4.4 Absolute Velocity of 1-Propanol Droplets Downstream of Throat Compared to Solid Sphere Model Predictions	48
4.5 Absolute Velocity of Ethanol Droplets Downstream of Throat Compared to Solid Sphere Model Predictions	49
4.6 Degree of Superheat Based on Pressure for Three Test Fluids	49
4.7a Degree of Superheat Based on Temperature for Three Test Fluids	50
4.7b Degree of Superheat Based on Temperature for Three Test Fluids	50
4.8 Normalized Ethanol Droplet Population Downstream of Throat	51
4.9 Normalized 1-Propanol Droplet Population Downstream of Throat	51
4.10 Normalized Hexanol Droplet Population Downstream of Throat	52
5.1 Evolution of Ethanol Droplet Absolute Mach Number, Relative Mach Number, Airflow Mach Number and Solid Sphere Mach Number With Distance Downstream of Throat	61
5.2 Evolution of 1-Propanol Droplet Absolute Mach Number, Relative Mach Number, Airflow Mach	

Number and Solid Sphere Mach Number With Distance Downstream of Throat	61
5.3 Evolution of Hexanol Droplet Absolute Mach Number, Relative Mach Number, Airflow Mach Number and Solid Sphere Mach Number With Distance Downstream of Throat	62
5.4 Normalized Static Pressure Without and After Detached Bow Shock for Ethanol Droplets	62
5.5 Normalized Static Pressure Without and After Detached Bow Shock for 1-Propanol Droplets	63
5.6 Normalized Static Pressure Without and After Detached Bow Shock for Hexanol Droplets	63
5.7 Degree of Superheat Based on Static Pressure Behind Normal Shock for Three Test Fluids	64
5.8 Degree of Superheat Based on Static Temperature Behind Normal Shock for Three Test Fluids	64
5.9 Relative Mach Numbers of Ethanol, 1-Propanol, Hexanol, and Solid Sphere Relative Mach Number vs. Distance Downstream of Throat	65
5.10 Weber Number vs. Downstream Distance	65
5.11 Reynolds Number vs. Downstream Distance	66

LIST OF TABLES

Table Number	Page
2.1 Test Fluid Properties	30

GLOSSARY

English

a	acceleration
D	diameter
F	force
Fo	Fourier number
K	drag coefficient
Oh	Ohnesorge number
P	pressure
S	degree of superheat based on pressure
St	Stokes number
T	temperature
t	time
v	velocity
We	Weber number
x	position downstream of throat

Greek

α	thermal diffusivity
Δ	change
ΔT	degree of superheat based on temperature
μ	viscosity
ρ	density

σ surface tension

Subscripts

c critical

D drag

d droplet

f final

i initial

jet jet

max maximum observed

r relative

sat saturation

v vapor

0 initial

∞ freestream

PREFACE

The views expressed in this article are those of the author and do not reflect the official policy or position of the United States Air Force, Department of Defense, or the U.S. Government.

ACKNOWLEDGEMENTS

The author would like to thank: Capt Jason Wolf for sparking interest in aeronautical engineering; Col Neal Barlow, LtCol Keith Boyer, and Dr. Julie Albertson for encouragement and support in applying to graduate school; Prof. Jim Hermanson for funding the research, and project guidance throughout the graduate school process; the Air Force Institute of Technology (AFIT) for the opportunity to attend graduate school as a first assignment; Maj Brad Thompson and Capt Nick Grauer for providing guidance and support as AFIT Liaison Officers; Col Phil Hamm, LtCol John Bowser, and LtCol Ian "Rocky" Sullivan for professional advice; family and friends for support and counsel through graduate school; and Jessica Koury for selfless dedication, support, and encouragement throughout graduate school, which moderated difficult times by illustrating dreams for the future.

INTRODUCTION

Aerospace propulsion has been an area of tremendous growth over the last century, however there is a gap in the capabilities of current engine design in the hypersonic regime. Engines employing turbomachinery, having been the most developed, are well understood, but have a limitation that they are only effective at low Mach numbers, below Mach 3.2. The reason is that the airflow into the engine must be slowed to subsonic speeds before reaching the compressor. Similarly, ramjet engines, although not containing turbomachinery, must slow the airflow to subsonic speeds before it enters the combustor section. This limits the maximum Mach number where ramjet engines are effective to about $M=5$. These engines do however require high-velocity ram air for their compression, making them ineffective at low Mach numbers.¹ Fortunately, there is overlap between turbo machinery engines and ramjets, making propulsion at all Mach numbers less than $M=5$ possible. Above Mach 5 however, there is only one choice in current use for propulsion, a rocket. Rockets require high flow rates of fuel and oxidizer, making them economically inefficient.² The most promising type of engine to fill the gap between Mach 5 and Mach 10 is a

supersonic combustion ramjet or scramjet.³ Bridging this Mach number gap through development of scramjet engines offers many advantages to the aerospace field. Not only would this allow for higher-velocity atmospheric vehicles, but it might also be employed as a hybrid with a rocket to give more efficient and less expensive access to space.²

Current developmental scramjet engines use liquid hydrogen or preheated hydrocarbon fuel because the airflow residence time in the combustor is very short at supersonic velocities.⁴ Hydrogen is attractive because it has a shorter autoignition delay and higher reaction rate than hydrocarbons for which the residence time of the fuel-air mixture in the combustor can be less than the autoignition delay.⁵⁻⁶ Unlike hydrocarbon fuels, liquid hydrogen is readily vaporized in the combustion chamber because it is cryogenic.² Also, compared to hydrocarbons, hydrogen molecules have far less mass, allowing the exhaust to reach higher velocities for a given combustion temperature. The major disadvantages to using liquid hydrogen as a fuel are that it is not storable, has a low energy density, and there are a lot of potential safety hazards associated with its use.² Current challenges associated with developmental

scramjet engines include flame stability, mixing, and combustion efficiency.

Hydrocarbon fuels may offer a solution to the problems associated with using hydrogen as a fuel for scramjet engines, making hydrocarbons more attractive for atmospheric flight and space launch. Additionally, hydrocarbons have a higher energy density than hydrogen, which would reduce structural mass and size requirements for a vehicle employing a scramjet.

One specific problem in using hydrocarbon fuels is that their autoignition delay time is long compared to hydrogen, requiring longer combustion chamber residence time and length. To overcome this obstacle, the hydrocarbons can be preheated through a heat exchanger. This would lower the autoignition delay time^{6,7} and could lead to the fuel being a source of cooling for the engine, especially if fuel were catalytically cracked.⁸ Unfortunately, this may require the use of either a bulky heat exchanger⁴ or dangerously volatile starter fuels.¹ Also, reliance on preheating the fuel may lead to complications in a flame-out situation requiring an "air start" where the heat in the engine is rapidly dissipated

by airflow and the fuel cannot be preheated to a necessary level for combustion.

Additionally, there are advantages to using an unheated liquid fuel. If a scramjet could be made to operate using an unheated liquid fuel, no specialized equipment would be needed in a "cold start" situation.⁹ Also from a mixing standpoint, liquid fuel injection would have a higher momentum than vapor, allowing the fuel to penetrate farther into the cross flow¹⁰ for better and more uniform fuel distribution. Superheating the liquid at injection may have potential to achieve rapid vaporization,¹¹ lowering the auto ignition delay, while maintaining the other advantages of liquid fuel injection.

To better understand the vaporization of liquids, numerous studies have examined the vaporization of individual droplets.⁹ Many of these studies have examined the aerodynamic shattering of the droplets and defined the mode and time to disruption in terms of various non-dimensional parameters.¹²⁻³⁰ The most popular of these parameters is the Weber number:

$$We = \frac{\rho_{\infty} \cdot v_r^2 \cdot D_0}{\sigma} .$$

The Weber number relates the external aerodynamic forces to surface tension. The Reynolds number is also very popular in defining different types of breakup:

$$Re = \frac{\rho_{\infty} \cdot v_r \cdot D_0}{\mu_{\infty}}$$

This parameter relates the external forces to the viscous forces. Finally the Ohnesorge number is often referenced:

$$Oh = \frac{\mu_d}{\sqrt{\rho_d \cdot \sigma \cdot D_0}}$$

The Ohnesorge number relates viscous forces to surface tension.

Through these studies, various aerodynamic modes of breakup have been identified.^{12-15,30} The most common modes are vibrational, bag, piercing, stripping, and catastrophic. The emergence and evolution of these modes is largely speculated to depend on the Weber number as shown in Fig. 1.1 below. This figure summarizes previous findings on aerodynamic breakup of droplets based on Weber number, and the type of test conducted. The piercing mode is not illustrated but was determined to exist between bag and shear stripping by the research of Theofanous *et al.*³¹ The research of Theofanous *et al.* also provides a visual

depiction of how the droplets disrupt in the different modes.

There have been few studies to focus specifically on the smooth application of aerodynamic loads to droplets in high-speed compressible conditions similar to what may be found in the combustor section of a scramjet engine. Most previous studies have focused on a steady application of aerodynamic loads to droplets at low subsonic speeds¹⁵⁻¹⁹ or sudden application through the use of shock tubes.^{12-13,20-26,29} These studies are insufficient in understanding the breakup of droplets in a high speed environment as the rate of aerodynamic loading and the speed of the flow have a strong effect on the breakup of droplets.^{12-13,27-28} Shock tube experiments inevitably lead to a "shock processing" of the droplet not necessarily experienced by a droplet of fuel injected into a supersonic combustor.

Additionally, most studies have ignored thermodynamic effects on the disruption of the droplets. The test fluids used to determine the modes of aerodynamic breakup presented in Fig 1.1 were non-volatile, meaning that they did not experience superheat, whereas a volatile fuel droplet in the same flow conditions would. One study, conducted on droplets at high subsonic velocities suggested

that superheating the droplets increases the violence of the breakup for a given value of Weber number.⁹ Based on this, droplets with a higher degree of superheat should have a shorter lifetime.

Results from earlier studies are varied, but suggest a rough idea of the type of breakup that may be encountered in a smooth application of aerodynamic loads up to moderate supersonic velocities. Fig. 1.2 shows the four droplet breakup regimes in a Mach 3 airflow, and suggests boundaries for the modes based on Weber number.³¹ This figure does display the piercing mode. The Weber numbers corresponding to these results are similar to those used in the present research, however these results only address the aerodynamic effects and ignore the influence of superheat, as the fluids tested again were non-volatile.

While categorizing the type of droplet breakup expected will help to define the transition from liquid fuel to vapor in a supersonic airstreams, understanding the velocities achieved by the droplets, time to vaporization, and combustor residence time is the main goal in advancing liquid fueled scramjet design. Droplet velocities and residence time are dependent on the drag force applied to

the droplets, however few studies have investigated the drag on droplets in supersonic flow.

The current research investigates the acceleration and maximum Mach number achieved before disruption by drops smoothly accelerated to supersonic velocities by forces imposed by the supersonic airflow. In this research, the airflow Mach numbers were much higher than the droplet Mach numbers, so the relative Mach numbers experienced by the droplets were greater than 1. Through high-speed multiple exposure images the velocity and acceleration of the droplets were calculated for various test fluids with a range of vapor pressures in a freely expanding jet test section of a draw-down supersonic wind tunnel. The results are then compared to a model of the droplets as rigid, non-deforming, non-evaporating solid spheres subject to the same airflow.

All three fluids are subject to the same aerodynamic loads, but their degree of superheat is different. One of the primary goals of this research is to determine the effects of superheat on droplet acceleration, velocities and lifetime, while keeping the Weber number, and therefore the breakup mode, relatively constant. It is expected that ethanol, with a higher degree of superheat will have a

shorter lifetime than 1-propanol and hexanol respectively. However, the ethanol and 1-propanol, having a significant degree of superheat, should experience more severe and faster breakup than the hexanol or predicated by previous studies of non-volatile liquids.⁹ Of interest is how superheat specifically affects the velocity, acceleration, and lifetime of droplets in supersonic airflow.

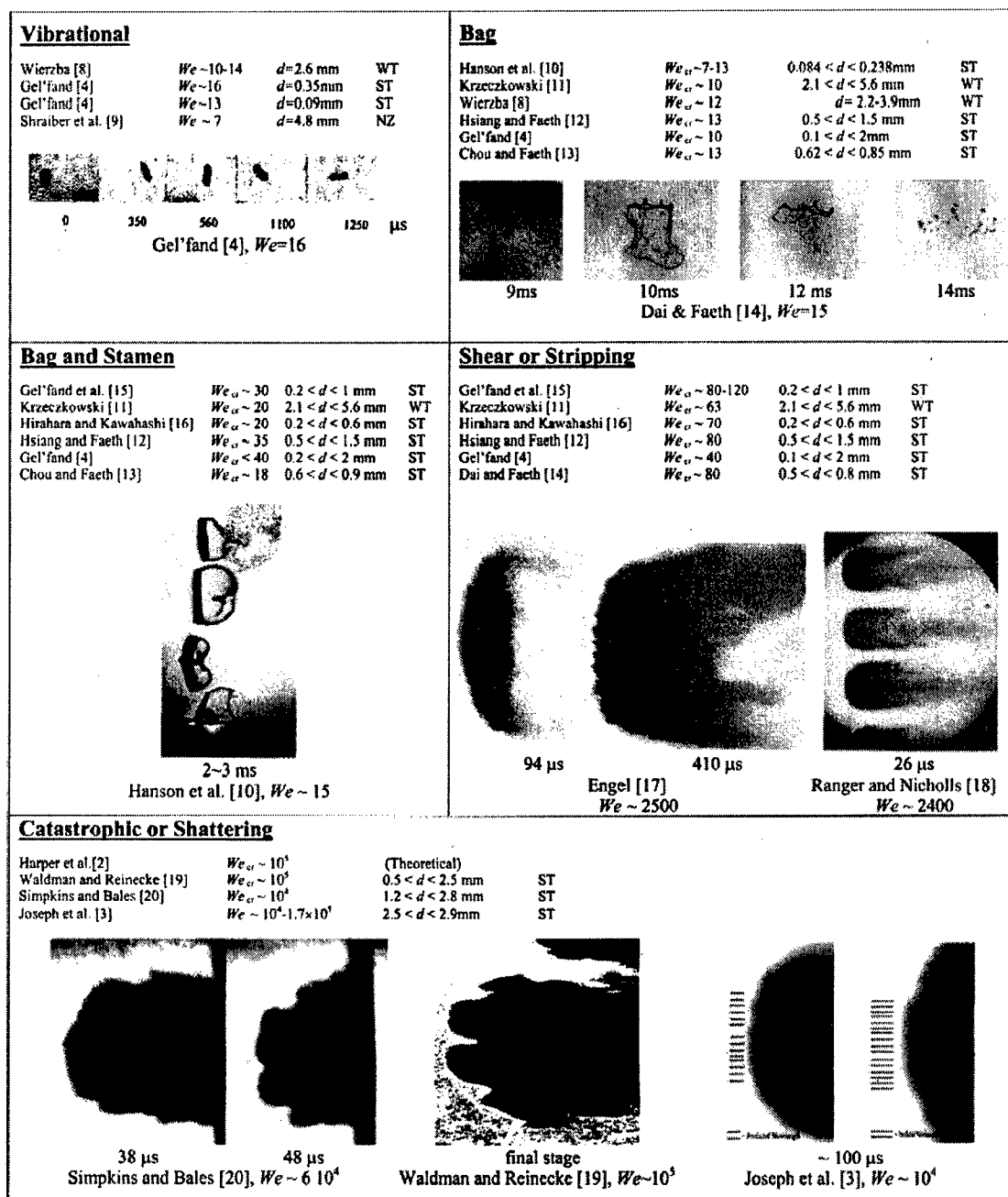


Fig. 1 Breakup regimes obtained at or near atmospheric conditions. All experiments were carried out at subsonic or mildly supersonic flow conditions. ST—shock tube, WT—Wind tunnel, NZ—Nozzle

Figure 1.1 Droplet Breakup Modes for Non-Volatile Droplets³¹

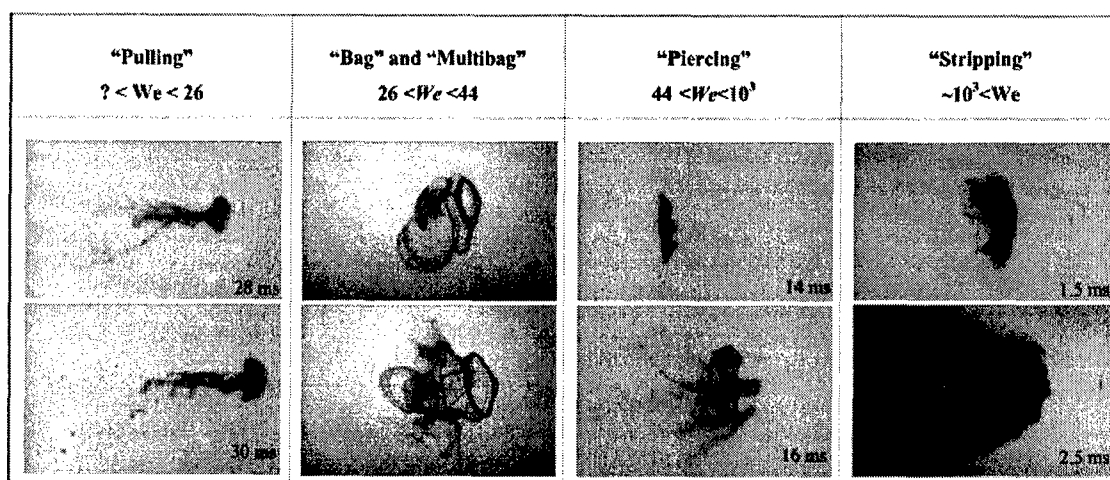


Figure 1.2 Classification of Breakup Mode Based on Weber Number for Non-Volatile Droplets in Mach 3 Airflow³¹

EXPERIMENTAL SETUP

Wind Tunnel

The experiments were conducted at the University of Washington in the draw-down Supersonic Wind Tunnel. This tunnel had three main components, a vacuum pump, a vacuum chamber (tank), and a leg with a manual valve to connect to a test section and supply the vacuum tank. The vacuum pump maintained a chamber pressure of 8.27 kPa (1.2 psia) when operating in an atmospheric pressure of 101.35 kPa (14.7 psia). A vacuum chamber, 30 m³ in volume, evacuated by the vacuum pump, was used to supply a constant vacuum during test runs. On the outside of the chamber a leg is attached which allows the test section to be mounted to the vacuum chamber. There is a manual valve on the top of this leg. When open, this valve allowed ambient air to be drawn through the test section and into the vacuum chamber.

Test Section

The test section was a small rectangular box mounted on the top of a PVC elbow that connects to the leg of the wind tunnel. A photograph of the test section and elbow are shown in Fig. 2.1. Four circular quartz windows with diameters of 40 mm (1.57 in) were mounted on the four sides

of the test section to allow for optical access. At the top of the test section was a circular interchangeable nozzle. The nozzle used in these experiments was convergent only (i.e., no divergent nozzle) to allow for a free expansion of the supersonic jet in the test section. This nozzle was chosen because it allowed for the most rapid flow acceleration in the test section. The convergent shape is a right conic frustum. The nozzle has a height of 15.875 mm (0.625 in), an entrance diameter of 25.4 mm (1 in) and a throat diameter of 3.175 mm (0.125 in). A picture of the test section is shown in Fig. 2.2 and a diagram of the test section and throat giving dimensions is shown in Fig. 2.3.

When the valve on the vacuum chamber arm was open, air flowed down through the nozzle, accelerating to Mach 1 near the throat, and further accelerating through free expansion in the test section to a maximum value of Mach 3.93. Pitot pressures were measured along the centerline by inserting a pitot probe through the bottom of the PVC elbow and measuring pitot pressures from the throat to the bottom of the test section. From these pressures, the Mach number, velocity, static temperature and static pressure were calculated as a function of distance downstream of the

throat. Figures 2.4-2.7 show these flow properties, respectively. The figures also show the location of the Mach disk, where the flow slowed due to a terminal normal shock. As a result of the discontinuities associated with the Mach disk, information provided downstream of the Mach Disk in Figs. 2.4-2.7 is inaccurate. The Mach disk location was located optically through Schlieren imaging. Fig. 2.8 displays the Schlieren photograph used to determine the position of the Mach disk, which was determined to be 10.88 mm (0.428 in) ± 0.23 mm (± 0.009 in) downstream of the throat.

Droplet Generation System

A *MicroFab* Droplet-on-Demand (DoD) device, pictured in Fig. 2.9, was used to generate 70 μm (0.0028 in) monodisperse droplets of the three test fluids. Fig. 2.10 shows the physical dimensions of the DoD device. This device required a voltage pulse and a steady supply of the test fluid to operate. A *MicroJet III* controller was used to supply a voltage pulse to the (DoD) device which caused a piezoelectric transducer in the device to create an acoustic wave in the fluid filled tip. This wave interacted with the free surface at the end to create a single drop per pulse.^{9,32} A steady fluid supply was

provided through the use of a pressure/vacuum system described in the next section. With a steady voltage pulse and supply of the test fluid, the DoD device generated a steady stream of droplets at 1000 Hz at the tip, 1 inch above the convergent entrance to the nozzle. This frequency was not high enough to cause significant droplet-droplet interaction, because the droplets were separated by roughly 3 droplet diameters at injection. 3-axis microstagers were employed in the mounting of the DoD device to allow for accurate alignment of the droplet stream with the centerline of the throat.

Liquid Supply System

Fluid supply to the DoD was accomplished by pressurizing a reservoir containing the test fluid, forcing the fluid through a 2-micron filter and then a Teflon capillary to the supply end of the DoD device. The pressure system utilized supply air at 15.5 psia, an analog regulator, and a small pressure vessel. Supply air first passed into the regulator, where the output pressure could be finely tuned. Next, it traveled to a half-gallon pressure chamber, and finally to the top of the fluid reservoir, forcing fluid out the bottom into the Teflon capillary. Precise tuning of the pressure was necessary

so a large-faced, analog pressure regulator was used.

There was also a hand-held vacuum pump attached to the pressure chamber. When the fluid reservoir needed to be refilled, the pressure was turned off and the bottom of the fluid reservoir was dipped in a pool of the test fluid. By pumping the hand pump, a slight vacuum was created in the reservoir and the test fluid was sucked into the reservoir. Figure 2.11 shows the supply system as it was utilized in the experiment. Fig. 2.12 is a cartoon of the supply system, provided for clarity.

When running experiments, the pressure was slowly increased to the point where fluid jetted out of the DoD device, and then the pressure was reduced as far as possible while still maintaining the jet. This purging technique eliminated pooling of the test fluid on the outside of the DoD tip and created a steady stream of liquid. When the voltage pulse was applied the stream was broken up into steady 70 μm diameter drops used in the experiment.

The shape, size and regularity of the droplets were verified during each test through back-illuminated direct photography with a Panasonic WV-CP474 CCD camera with a 105 mm f2.8 Nikkor lens. 480 x 640 pixel images were captured

by a *Mu-Tech* MV1000 PCI frame grabber card by a controlling PC which recorded the images as 8-bit grayscale TIFF images on the PC hard drive for verification purposes. Only the space between the tip of the DoD device and the entrance of the nozzle was visible in the field of view, so the form of the droplets could be verified before they were affected by supersonic airflow. Illumination was accomplished with a Xenon Corp. N989B Nanopulse system (500 mJ (0.12 cal) per 10 ns pulse) triggered by the *MicroJet III* controller at a rate of 1000 Hz so that the lamp fired every time a droplet was released. During the 10 ns pulse width a droplet moving at 40 m/s (the average droplet speed measured just downstream of the throat) traveled only 0.5% of its diameter. The actual velocities above the throat were much less than the velocity at the throat, meaning that the drops only moved a fraction of their diameter during the pulse duration allowing them to be effectively "frozen" in the pictures. With the light source mounted opposite the camera lens beyond the droplet stream, the droplets were clearly visible so that their size and regularity could be verified prior to entering the test section. Fig. 2.13 shows a sample of an image taken with the Panasonic camera.

Droplet Imaging System

Imaging of droplets and velocity measurement in compressible flow was accomplished using a Princeton Instruments PI Max 2 ICCD camera with a VZM 300 video microscope lens. The images were captured by a PCI card included with the PI Max 2 camera, and stored on a controlling computer's hard drive for post processing. Illumination for the data acquisition pictures was provided by a New Wave Research Solo PIV 120 Nd:YAG Laser. When triggered by a controlling computer using *Pixel Flow* software, the laser fired two pulses 10 μ s apart. Each pulse contained 400 mJ of energy with a duration of 5 ns. This method is similar to Particle Image Velocimetry (PIV), however, in this case the droplets did not follow the flow. This is confirmed by the Stokes number:

$$St = \frac{\frac{d_d^2 \rho_d}{18 \mu_d}}{\frac{d_{jet}}{2 v_{max jet}}}$$

1-propanol was used to calculate a representative value of the Stokes number for these experiments. The result was $St=0.84$, which indicates that the droplets do not follow the flow, as would be the case for $St \ll 1$. Each image

captured only 2 flashes of the laser light. At the highest measured velocities, 140 m/s, droplets moved 280 nm or 10% of their original diameter during the 5 ns pulse width so they were effectively frozen in the pictures. A two-lens optical system was used to form the laser light into a vertical sheet. At the centerline of the test section, the laser sheet was 50 mm (1.97 in) tall and 2 mm (0.078 in) wide. The width of the laser sheet was kept as thin as possible to insure that only droplets falling along the centerline were illuminated by the light. In the other dimension, the distance of the droplets from the centerline could be measured from the images. Data points were only taken from droplets that fell within 1 mm (0.039 in) from the centerline to insure that the maximum variation from the centerline for all data points was less than 1 mm.

The imaging sequence originated with a trigger pulse from a controlling computer, opening the shutter for the camera. After 20 μ s had passed, the controlling computer fired the first laser pulse, and 10 μ s later the second laser was fired. Finally 50 μ s after the trigger signal the camera shutter was closed. Figure 2.14 shows the triggering sequence used in data acquisition. The whole

process was repeated at 12 Hz for the duration of the experiments.

The resulting images contained multiple exposures of the droplets in supersonic airflow. By also imaging a scale, the distance per pixel could be calculated. By measuring the pixel distance in the multiple exposure images, multiplying by the distance per pixel and dividing by the 10 μ s delay time, the velocities of the droplets imaged were found. The field of view in all of the images varied slightly because of slight adjustments to re-focus the lens, however the maximum downstream distance was 0.016m (0.63 in). Very few droplets survived breakup beyond this point, therefore there was no need to extend the field of view further downstream. To streamline data calculations, pixel coordinate pairs were entered into an Excel spreadsheet to calculate velocities. Each pixel traveled by the droplets represented a velocity increase of 3.29 m/s. The centers of the droplets were measured to an accuracy of ± 1 pixel each, so the calculated velocities have an error of 6.59 m/s (21.59 ft/s) or about 7.3% of the mean maximum velocity.

Test Fluids

The test fluids used in this study were ethanol, 1-propanol, and hexanol. Table 2.1 outlines some of the physical properties for these fluids including their Ohnesorge numbers. These fluids were chosen because of their similar densities and surface tensions, with the primary difference being their vapor pressures. Maintaining similar surface tensions ensured that the Weber numbers for droplets of the same size and velocity were very similar, minimizing the variation in the aerodynamic breakup modes between the three fluids.

Varying vapor pressure allowed for different degrees of superheat in the liquids at injection, which has been suggested to amplify the effects of aerodynamic breakup.⁹ Categorizing the effects of superheat on the disruption of liquid fuel droplets in supersonic flow was the primary goal of this research.

Data Processing

A *Matlab* code was used to read data from the Excel spreadsheet and further process the data. The *Matlab* codes combined information from the Excel velocity

calculations and the centerline Mach number measurements to calculate Mach numbers, relative Mach numbers, and relevant physical airflow properties affecting the droplets. The degree of superheat can be defined based on the vapor and air pressures:

$$S = \frac{P_v}{P_\infty},$$

For a given ambient static pressure, it was expected that ethanol would have the highest level of superheat, and conversely hexanol the lowest. In these tests, superheating was accomplished by exposing the room temperature liquid droplets to pressures below their saturation vapor pressure at room temperature due to the rapid decrease in pressure in supersonic flow. Hexanol was the exception because the static pressures in the test section did not fall below its room temperature vapor pressure, so hexanol was not superheated. Alternately, superheat can be expressed as the difference between the temperature of the liquid and the saturation temperature of the liquid at a given pressure:

$$\Delta T = T_d - T_{sat}.$$

Given that the other properties suggested to influence droplet breakup are very similar, the difference in

superheat should translate into earlier breakup of the ethanol droplets than 1-propanol and hexanol. It should be noted that the fluid temperature in the bulk of the droplet was assumed to be constant. This assumption is backed by the Fourier number¹¹:

$$Fo = \frac{4 \cdot \alpha \cdot t}{D^2},$$

where t is the residence time of the droplets in the test section. The resulting value of $Fo \approx 0.01$ for all the test fluids suggests that cooling of the main droplet fluid is negligible in the supersonic flow because of the very short droplet lifetimes.¹¹

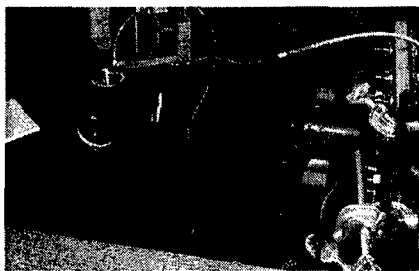


Figure 2.1 Test Section Mounted on PVC Elbow



Figure 2.2 Test Section Exterior

The image is 13.25 cm x 13.25 cm

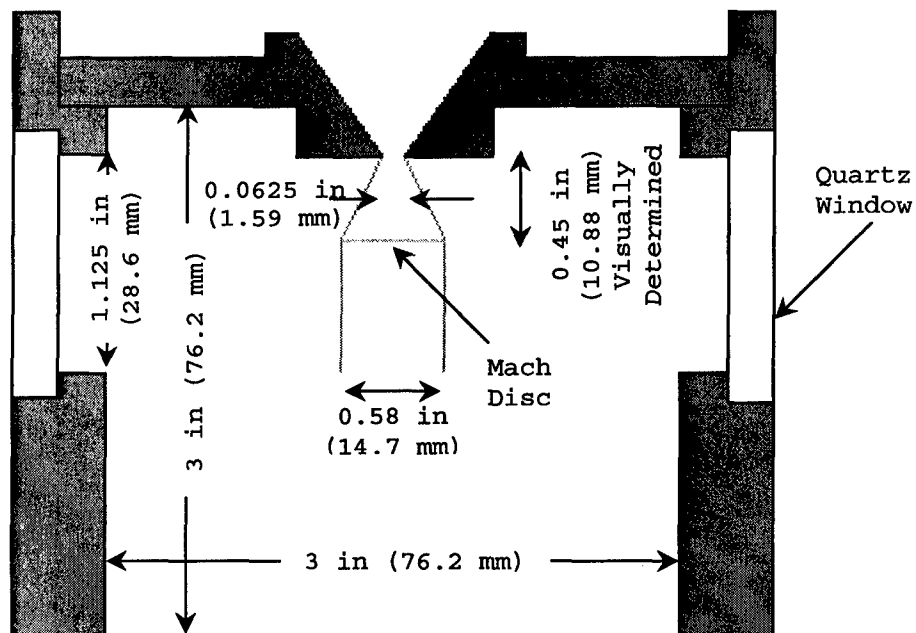


Figure 2.3 Test Section Interior

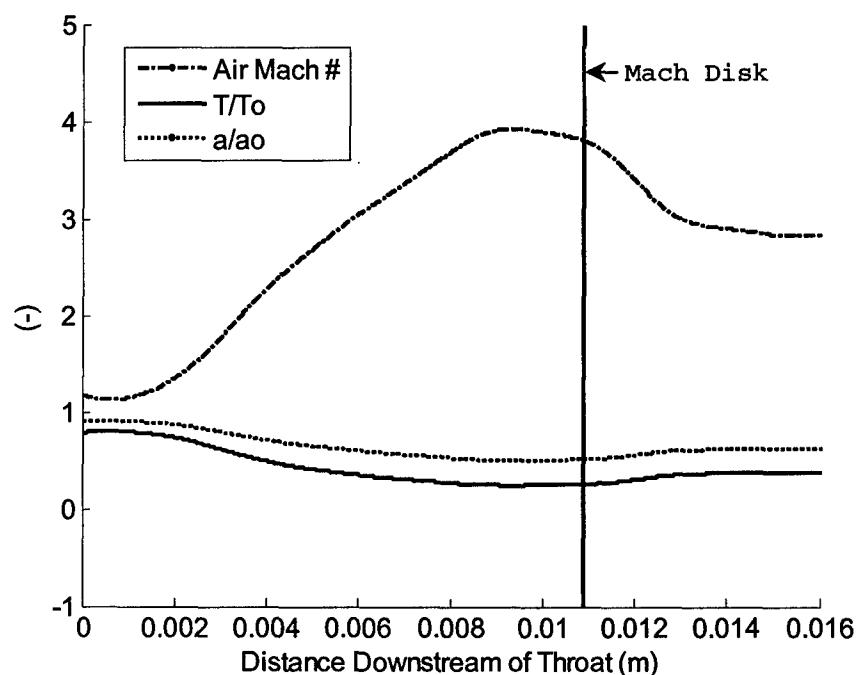


Figure 2.4 Centerline Mach Number, Normalized Static Temperature and Normalized Speed of Sound Determined From Pitot Probe Measurements

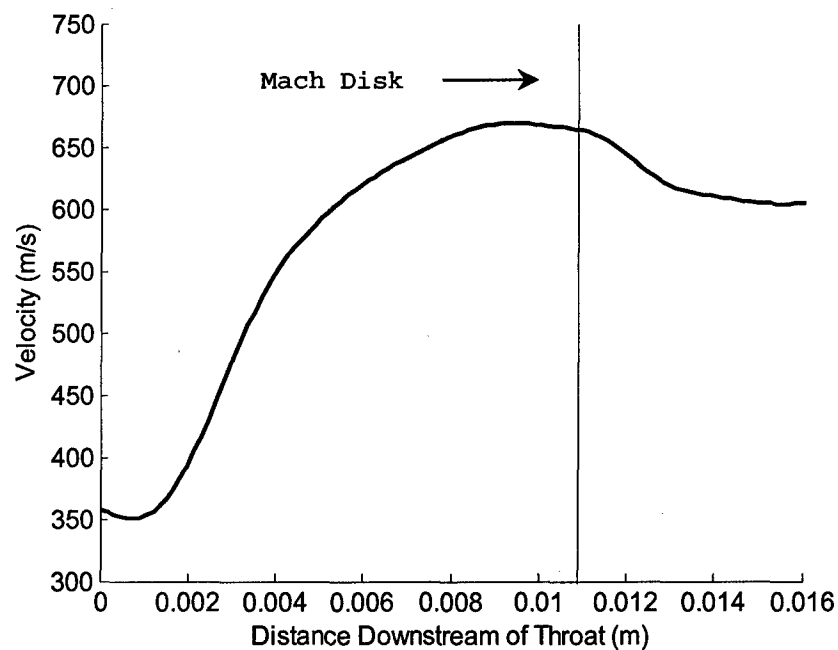


Figure 2.5 Centerline Air Velocity

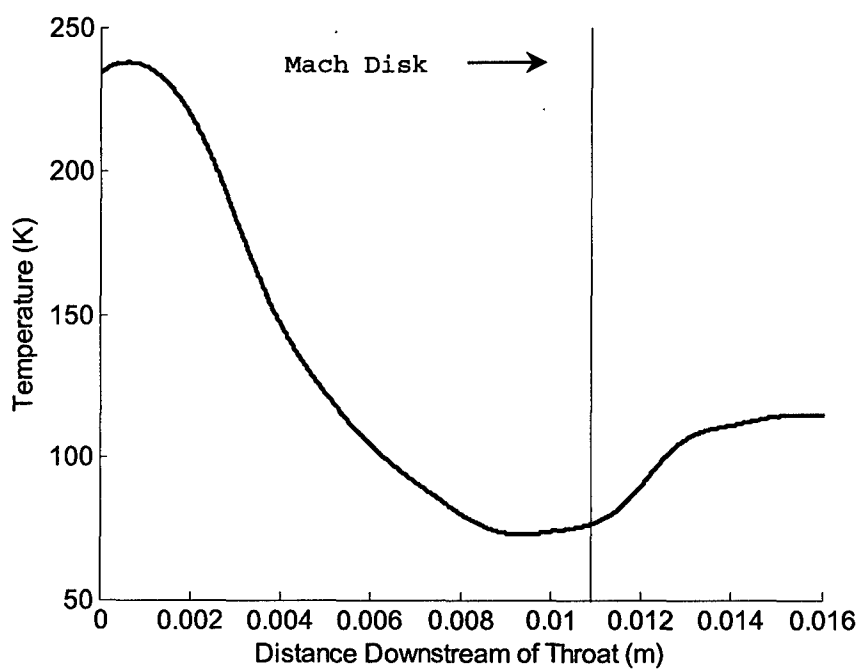


Figure 2.6 Centerline Static Temperature

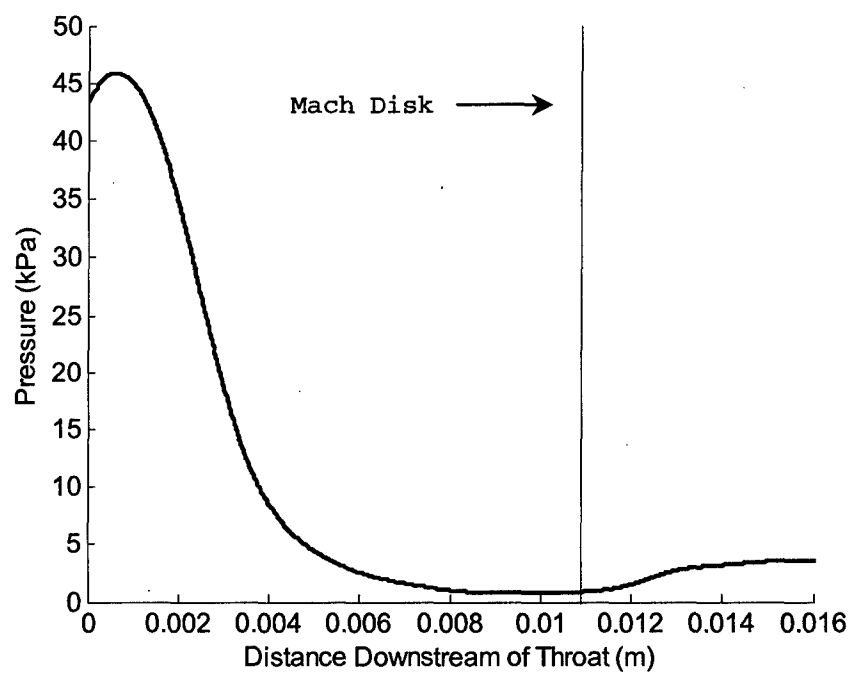


Figure 2.7 Centerline Static Pressure

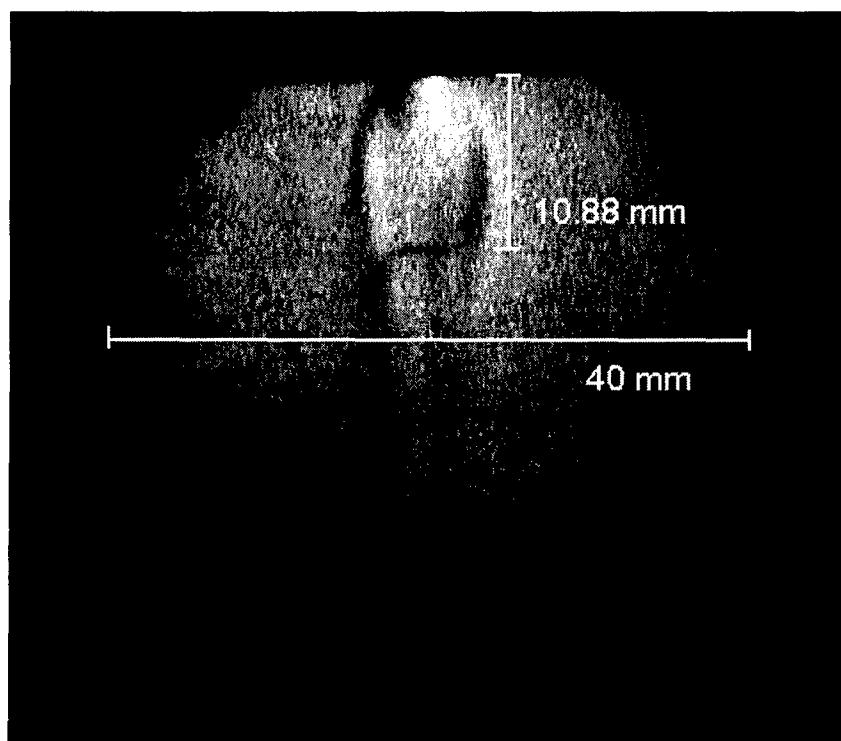


Figure 2.8 Mach Disk Schlieren Photograph



Figure 2.9 DoD Droplet Generator

The image width is 3.0 cm

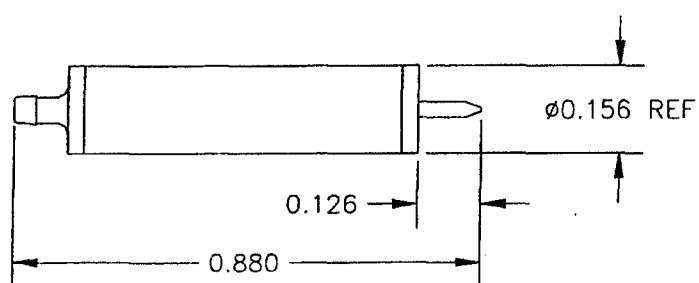


Figure 2.10 Physical Dimensions of DoD Device



Figure 2.11 Pressure/Vacuum Supply System

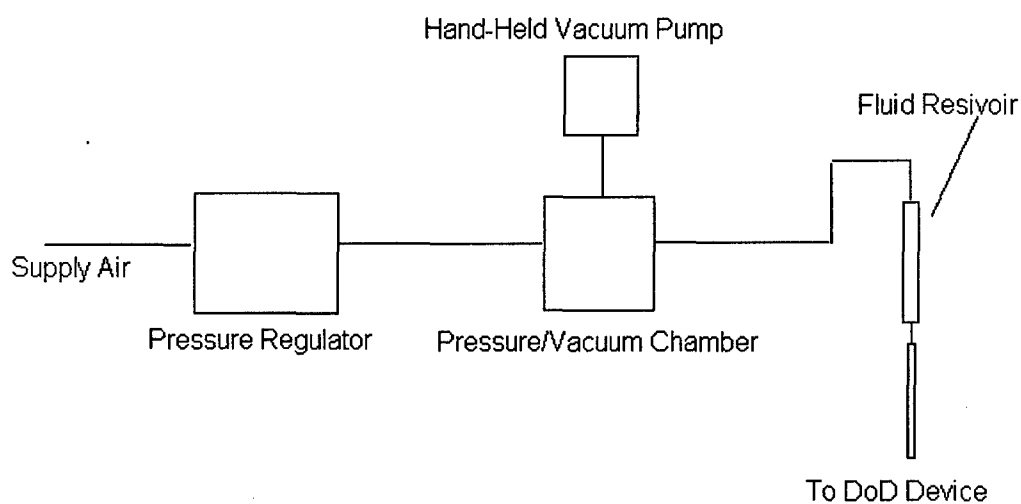


Figure 2.12 Diagram of Pressure/Vacuum Supply System

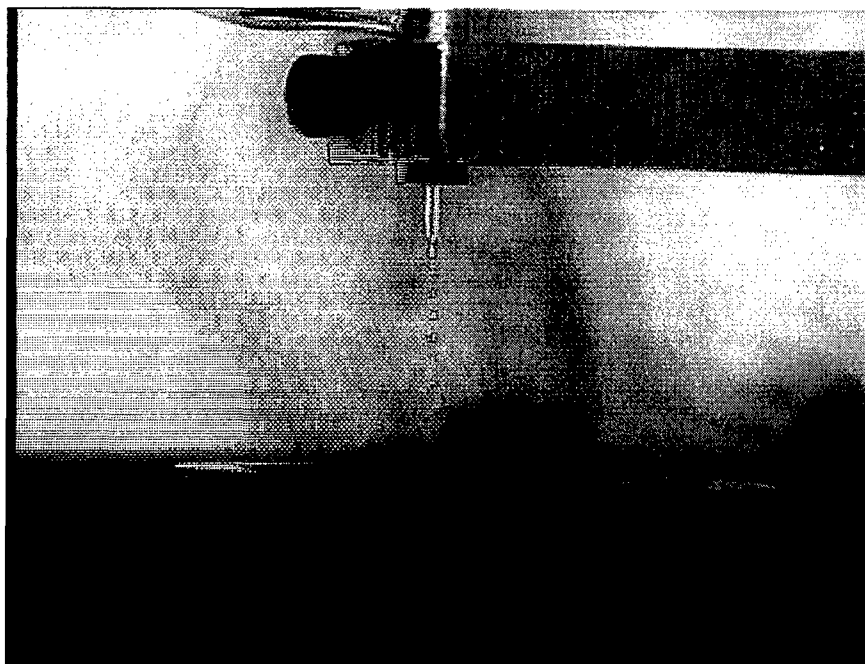


Figure 2.13 Sample Panasonic Camera Image Used Droplet Size and Spacing Verification

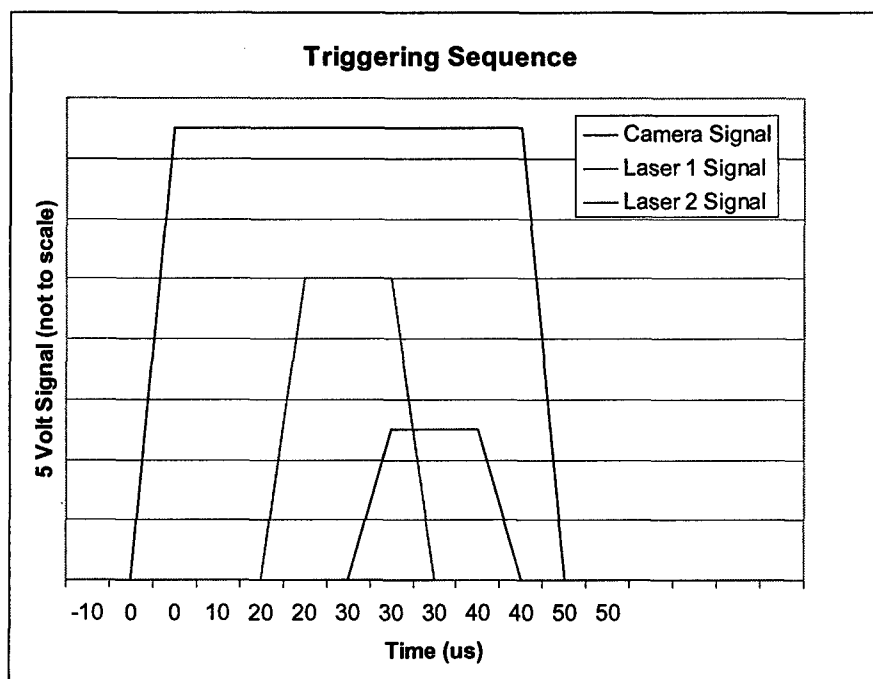


Figure 2.14 Triggering Sequence

Table 2.1 Test Fluid Properties

Test Fluid	P_v kPa	ρ g/mL	σ mN/m	μ cP	Oh	T_c K
Ethanol	7.916	0.792	21.97	1.17	0.0340	517.45
1-Propanol	2.88	0.783	23.32	2.26	0.0632	535.25
Hexanol	.016	0.812	25.81	5.40	0.1434	613.23

DROPLET ACCELERATION MODEL

In order to compare the experimental results to theory, a one-dimensional model of droplet acceleration and velocities was applied using drag approximations for a solid sphere.¹¹ This method was developed by Phariss¹¹ to estimate a value of Weber and Reynolds numbers to predict the type of droplet breakup expected. In this study it is used only for comparison of velocities and accelerations, as the Weber and Reynolds numbers were calculated from measured velocities. From the modeled velocities, relative droplet velocities were obtained by subtracting the centerline airflow velocities. The local speed of sound was then used to determine the relative droplet Mach number. These data were used to compare the actual measurements with what a solid sphere model would predict, to assess how the droplet disruption affects the drag on the droplets by the deviation from the model. This model was for a rigid, non-deforming, sphere, so it did not account for deformation, disruption, superheat or vaporization which all effect the liquid fuel droplets. Also, the model results were used to give an approximation of the droplet breakup regime that could be predicted for

the droplets, based on the observations of previous studies.^{12-14,16,20-22,29-30}

Model Structure

The model relied on an approximation of the liquid drops as non-evaporating, solid spheres. This assumption was necessary to use existing drag data on small-diameter metal spheres, measured at Mach numbers of 0.29 to 3.96.³³ Another limitation to the accuracy of this model is that the diameter of the metal spheres used to collect the drag data were larger than the diameters of the droplets. Also, the effects of compressibility on spheres of the scale of the droplets are not well understood. Presented are the values for the sphere coefficient of drag as a function of Mach number:

$$K_D = \begin{cases} 0.192 & , 0 < M < 0.5 \\ 0.3173 + 0.2711 \cdot (M - 1) & , 0.5 < M < 1.4 \\ 0.3812 - 0.0140 \cdot (M - 2.75) & , 1.4 < M < 4.0 \end{cases}$$

These coefficients are related to the drag force as follows:

$$F_D = K_D \cdot \rho_\infty \cdot D^2 \cdot v_r^2$$

The model was used to predict velocities of the droplets from the tip of the droplet generator through the

test section at increments of 1/160 in (0.159 mm) At the initial position step, the droplet velocity was assumed to be half of the airflow velocity. At each step the velocity was calculated and divided by the experimentally determined speed of sound to give the Mach number. Next, the difference between that Mach number and the measured air Mach number was taken as the relative Mach number to be used in the equation above. The force on the droplet was calculated using experimentally determined free stream density. Assuming a constant mass for a 70 μm diameter droplet at a free stream density, acceleration was calculated. Using the following equation, the Newtonian equation for change in velocity due to a constant acceleration over a distance, a new velocity was calculated for the next position step.

$$v_f^2 = v_i^2 + 2 \cdot a \cdot \Delta x$$

This process was repeated over each of the small position steps to give high resolution to the result. The density of ethanol was used because the densities of the fluids vary only slightly.

Model Results

According to the solid sphere model, droplets should accelerate from 322.8 m/s (1059 ft/s) at the throat to a maximum of 441.6 m/s (1448.65 ft/s) before decelerating relative to the airflow again. This is shown in Fig. 3.1. The relative Mach number is predicted to increase from $M=1.058$ at the throat to a maximum of $M=2.535$, as shown in Fig. 3.2. The predicted relative Mach number continues to increase after the predicted relative velocity peaks due to the speed of sound decreasing with the static temperature downstream of the throat.

Although the drag data were based on experiments for larger spheres than the droplets considered here, the Reynolds numbers predicted by the model fall into the range of smooth spheres in incompressible flow used in the studies to obtain the data.³⁴ This suggests that the drag coefficients used in this model are acceptable for the size of droplet modeled. Model Reynolds number data are presented in Fig. 3.3.

The results of the model provide a base to compare the experimental data. However, the experimental data was expected to differ from the model as a result of droplet deformation, disruption and vaporization.

Breakup Mode Predictions

Many previous studies have focused on the correlation between Weber number, Reynolds number and Ohnesorge number and the mode of breakup that droplets undergo. Although there is some variation in the correlations, there are likely two dominant modes for the values of the non-dimensional parameters in this study. Shear stripping disruption is expected, and transition to catastrophic disruption is possible as a result of large Weber numbers³¹ ($We \sim 725$).

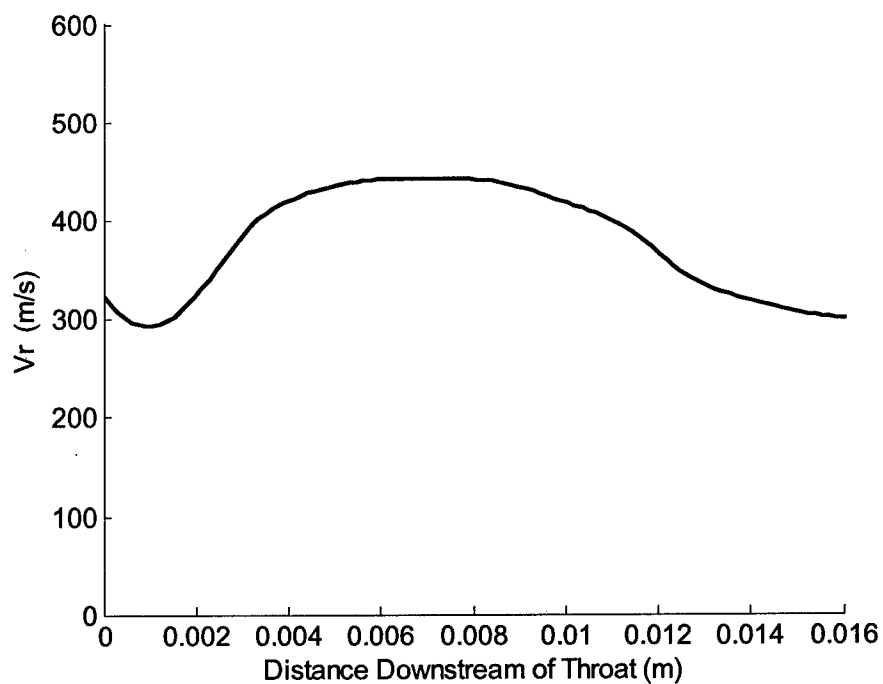


Figure 3.1 Modeled Droplet Relative Velocity

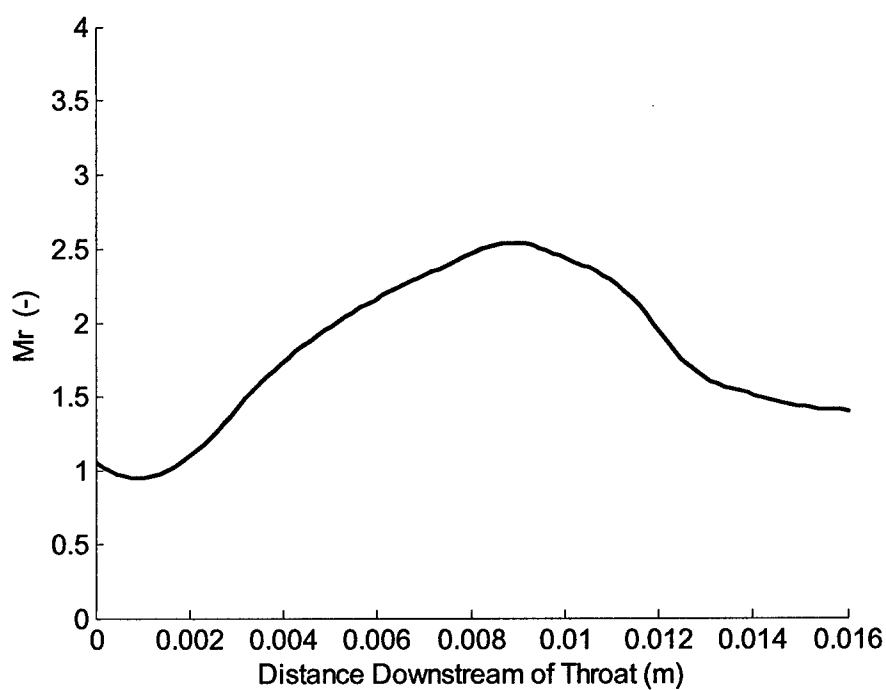


Figure 3.2 Modeled Droplet Relative Mach Number

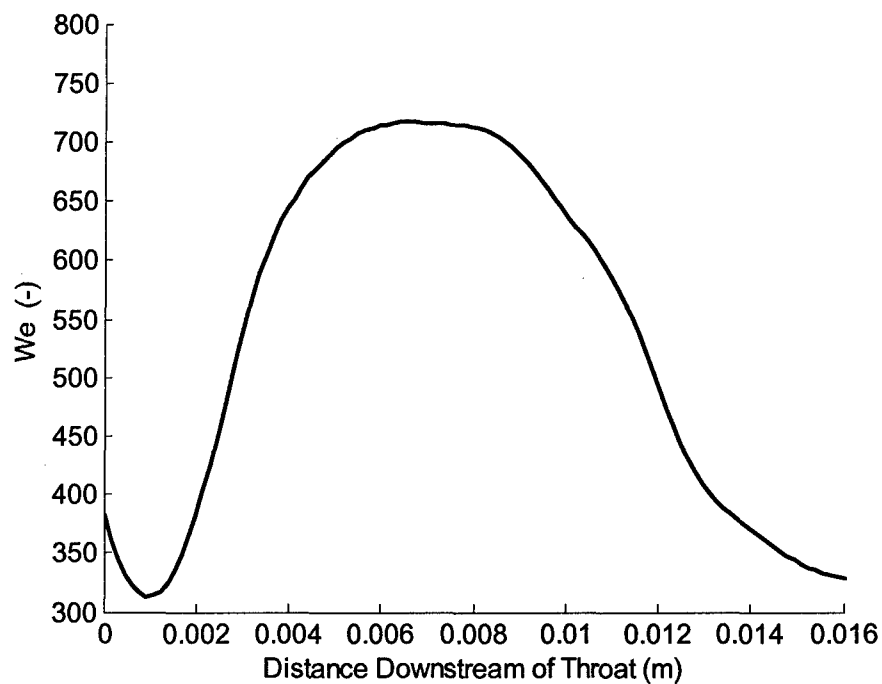


Figure 3.3 Modeled Droplet Weber Number

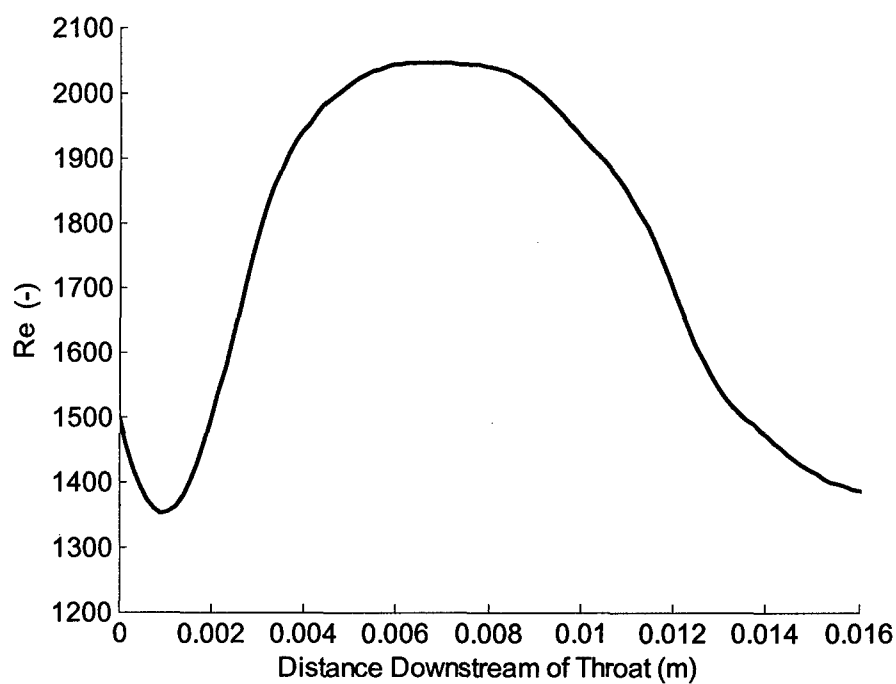


Figure 3.4 Modeled Droplet Reynolds Number

EXPERIMENTAL RESULTS

Droplets of the three fluids were imaged in test runs that each contained 250 images. A sufficient number of test runs for each fluid was made to produce at least 150 useable velocity measurements. For 1-propanol, approximately 10% of the acquired images were useable for velocity measurements. In contrast, for ethanol and hexanol, approximately 5% of the images were useable. Figure 4.1 shows a sample multiple-exposure image for 1-propanol droplets (and the measured velocities for the two image pairs shown). In this image the throat is at the top, with the bottom of the nozzle illuminated horizontally at the top, and the airflow is from top to bottom. Droplets for the three fluids were imaged from the nozzle exit to just beyond the Mach disk at a downstream distance of $x=0.011$ m (0.433 in).

The low-yield problems were due to the combined difficulties of getting the drops to fall exactly on centerline so that they would be illuminated by the laser sheet, and droplet disruption. As the airflow accelerated toward the entrance to the nozzle, currents in the airflow caused movement of the droplet stream, as observed visually. This problem was present in all of the test

runs. Results for droplets consisting of each of the three test fluids are discussed below.

Hexanol

Hexanol droplets were the most difficult of the three to image satisfactorily. This was unexpected because hexanol has a vapor pressure lower than the lowest vapor pressure present in the test section, and therefore should not be superheated and should be the most stable of the three test fluids. The hexanol droplets appeared to disrupt closer to the nozzle exit than the other liquids. The amount of mist and smaller droplets trailing the main droplet in the hexanol pictures suggests that these droplets may have been more subject to the aerodynamic stripping and breakup than the other liquids. Many of the hexanol droplet images taken did not accurately reflect the shape of the droplet due to the amount of droplet particles and mist surrounding the main droplet. This disruption was not expected as the Weber numbers just downstream of the throat are similar for all three fluids, with values between 350 and 400. It is possible that the viscosity of hexanol, roughly 2 times greater than that of 1-propanol, causes it to suffer from different breakup mechanisms. Increasing viscosity can significantly delay the transition

to stripping or catastrophic breakup based on Weber number.³¹ It is possible that the increase in viscosity caused the hexanol droplets to be subject to a different breakup mode than the droplets of the other liquids.

Figure 4.2 shows a sample image of a hexanol drop exhibiting early breakup. Great care was taken to only collect data points from the most composed droplets of hexanol, however that data set still had the largest variability of the three.

Figure 4.3 displays the absolute measured velocity as a function of downstream distance from the nozzle throat for hexanol. There is a high amount of scatter for the hexanol data, amounting to as much as 20% of the mean maximum measured velocity (the measurement uncertainty was estimated to be approximately 7%). The initial acceleration of the hexanol droplets was the least of the three fluids. The initial slope of the velocity curve shown in Fig. 4.3 suggests an initial droplet acceleration of $10,600 \text{ m/s}^2$. The hexanol droplets achieved the highest absolute measured velocities of the three fluids tested, approximately 92 m/s at the downstream limit of data collection $x=0.014 \text{ m}$. These trends are more visible in the

relative Mach number figures presented in the Discussion section below.

1-Propanol

The 1-propanol droplets provided the highest fraction of useable droplet images. The droplets were generally well-composed in the multiple-exposure pictures, and seemed to survive intact for a significant distance down the test section. This fluid is recommended for a calibration fluid in further experiments because of its fraction of useable images under these conditions. Figure 4.4 shows the absolute measured velocity of the 1-propanol droplets as a function of downstream distance from the throat. The slope of the velocity curve in Fig. 4.4 suggests an initial acceleration of $13,900 \text{ m/s}^2$, higher than was observed for the hexanol. The mean maximum absolute measured velocity of the 1-propanol droplets was approximately 90 m/s at the downstream limit of data collection $x=0.014 \text{ m}$, lower than the maximum velocity observed for the hexanol droplets. The 1-propanol data are clustered better toward the throat, but again there is significant variation in the data far downstream amounting to as much as 31% of the mean maximum velocity.

Ethanol

The ethanol droplets led to a lower fraction of useable images than 1-propanol droplets, but higher than that of hexanol droplets. As with the hexanol, many of the images were clouded by fragments as the droplets disrupted. Again, great care was taken only to select data points where the droplet seemed to be spherical and there were no fragments that would cause ambiguity in determining the center of the droplet. The resulting velocity data gave the least scatter of the three fluids with variation amounting to as much as 16% of the mean maximum observed velocity (the measurement uncertainty was estimated to be approximately 7%). Figure 4.5 shows the absolute velocity of the ethanol droplets as a function of the downstream distance from the throat. The maximum velocity observed for ethanol droplets was approximately 82 m/s, the lowest of the three fluids. These droplets also accelerated the fastest near the throat, with an estimated initial acceleration of 16,400 m/s².

The predicted velocity of the droplets if they were smooth, non-evaporating rigid spheres subjected to the same airflow conditions is also shown in Figs. 4.3-4.5. It should be noted that the predictions are fairly close to

the experimental data for distances downstream to about 0.0015 m, and after that diverge quickly. This suggests that initially the droplets start as spheres but the deformation due to aerodynamic and thermal loads, significantly changes their drag characteristics. The difference in the velocity profiles of the solid sphere model and those of the actual droplets indicates that the drag on the deforming droplets is in all cases significantly less than would be experienced by solid sphere in the same airflow.

As expected, the ethanol droplets were visually observed to disintegrate earlier than the other two fluids. Ethanol has the highest degree of superheat and the lowest viscosity of the three fluids. The higher degree of superheat experienced by the ethanol droplets was likely the reason for the more pronounced disruption of this fluid compared to the 1-propanol.

The degrees of superheat are shown in Figs. 4.6 and 4.7, with the reference static pressure being that of the airflow. Figure 4.6 shows the pressure based degree of superheat, and Figs. 4.7a and 4.7b show the difference between the liquid temperature and the saturation temperature at the airflow pressure. Additional saturation

temperature data were used to construct a model of saturation temperature for a given pressure for Figs. 4.7a and 4.7b.^{35,36} Figures 4.7a and 4.7b display the same information, but have different scales for emphasis on the positive degree of superheat. Figures 4.6-4.7b show that the ethanol droplets achieved a degree of superheat above that for the 1-propanol droplets. The hexanol droplets experienced negligible superheating.

Droplet Population

As mentioned earlier, the ethanol droplets disintegrated closest to the nozzle exit, followed by the 1-propanol and the hexanol droplets. To show this, population histograms were produced as a function of downstream distance from the throat. Figures 4.8, 4.9, and 4.10 show the ethanol, 1-propanol, and hexanol relative population data, respectively. In these histograms, the first two bins for each fluid contain large populations, but the populations downstream drop off in order of the highest vapor pressure to the lowest, with ethanol having the lowest population in the last bins, and hexanol having the highest. The more rapid decrease in population with downstream distance for the ethanol and 1-propanol is likely due to these fluids being superheated. The ethanol

and 1-propanol droplets disrupt more rapidly than those of hexanol causing a steep trend in the histograms compared to the more steady decline in population of hexanol droplets with downstream distance. The unexpected rise in the droplet population for the case of hexanol may be a result of not having enough data points to show a steady downward trend in the populations from the throat to the end of the test section.

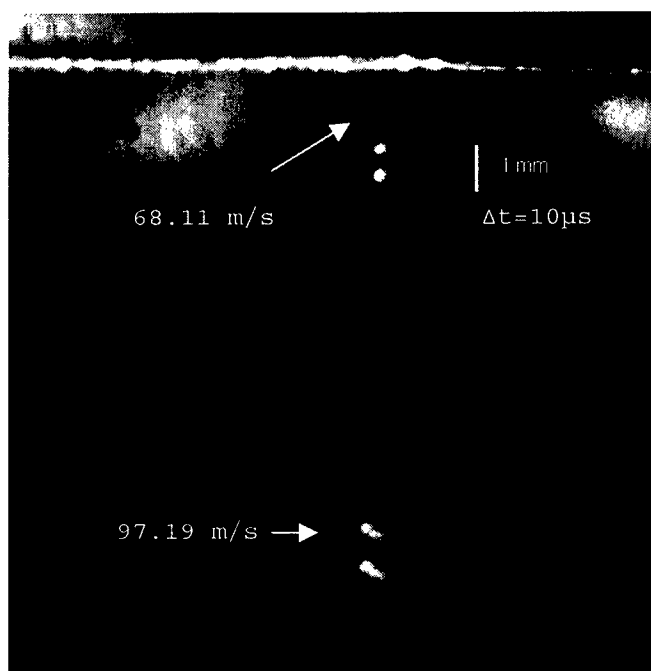


Figure 4.1 1-Propanol Droplet Multiple Exposure Image

The bright horizontal line is the plane of the nozzle throat, and the flow is from top to bottom

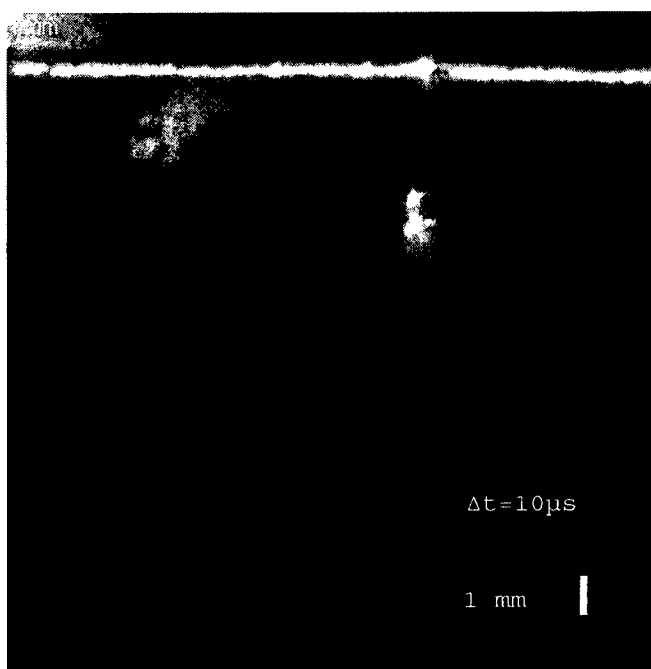


Figure 4.2 Hexanol Droplet Multiple Exposure Image

The bright horizontal line is the plane of the nozzle throat, and the flow is from top to bottom

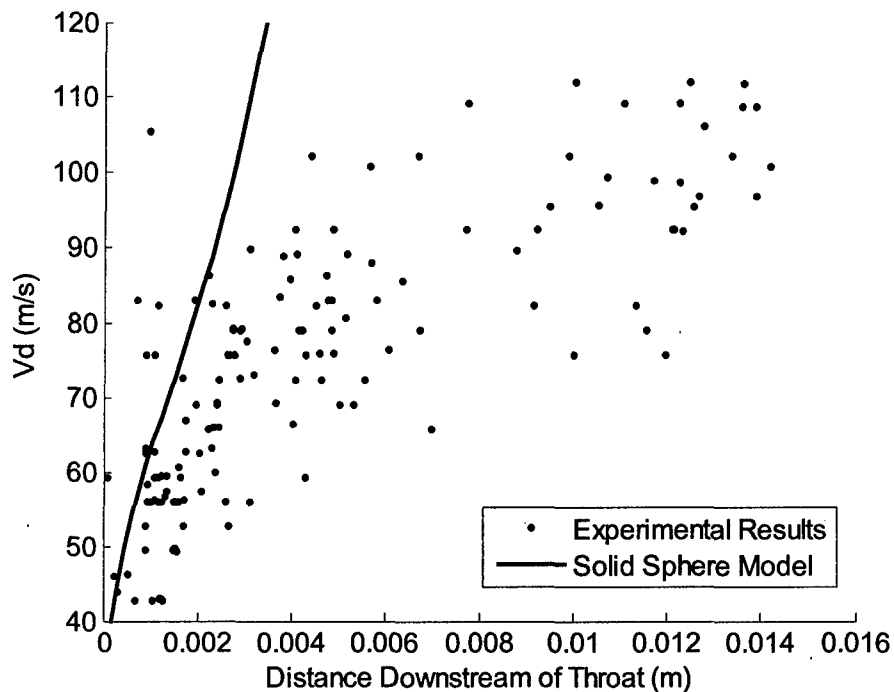


Figure 4.3 Absolute Velocity of Hexanol Droplets Downstream of Throat Compared to Solid Sphere Model Predictions

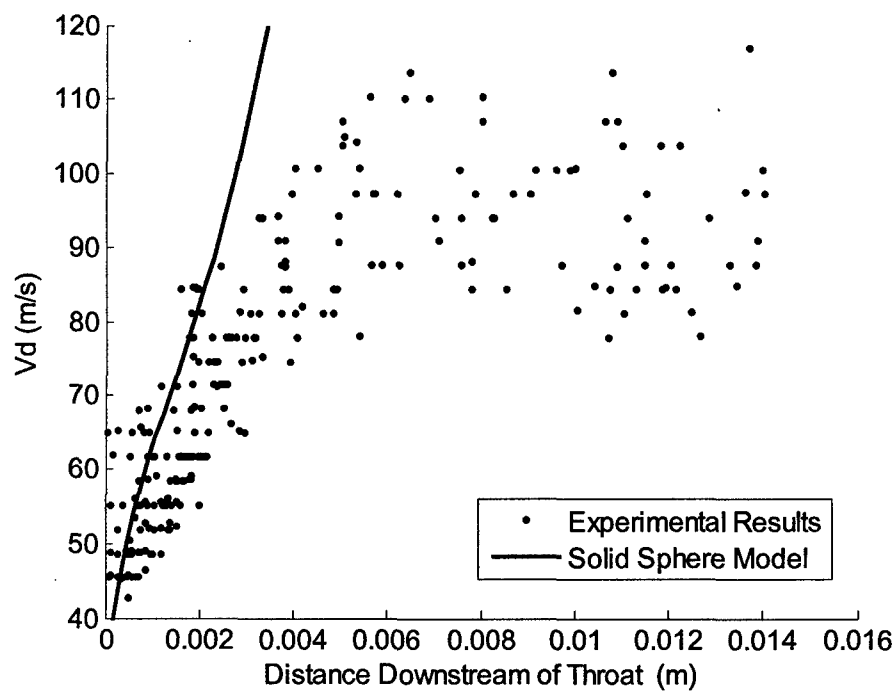


Figure 4.4 Absolute Velocity of 1-Propanol Droplets Downstream of Throat Compared to Solid Sphere Model Predictions

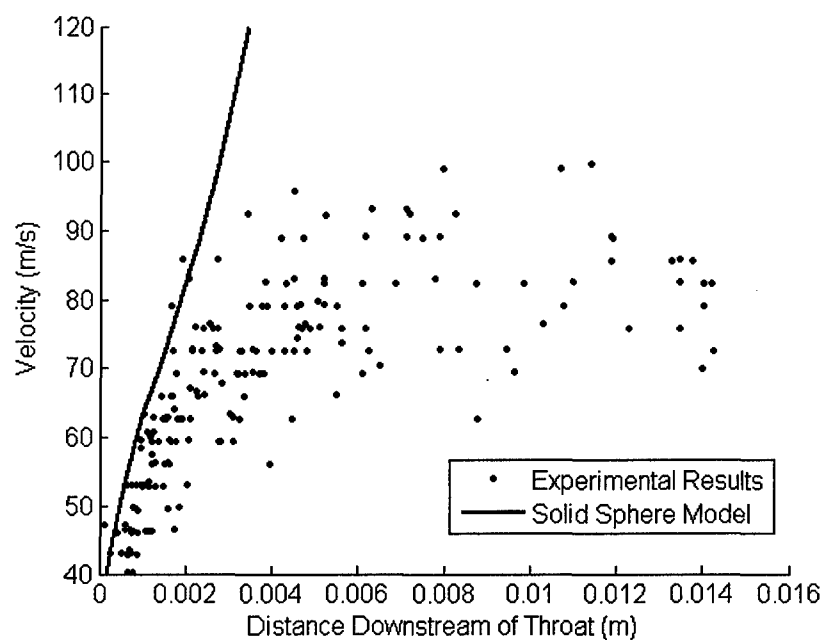


Figure 4.5 Absolute Velocity of Ethanol Droplets Downstream of Throat Compared to Solid Sphere Model Predictions

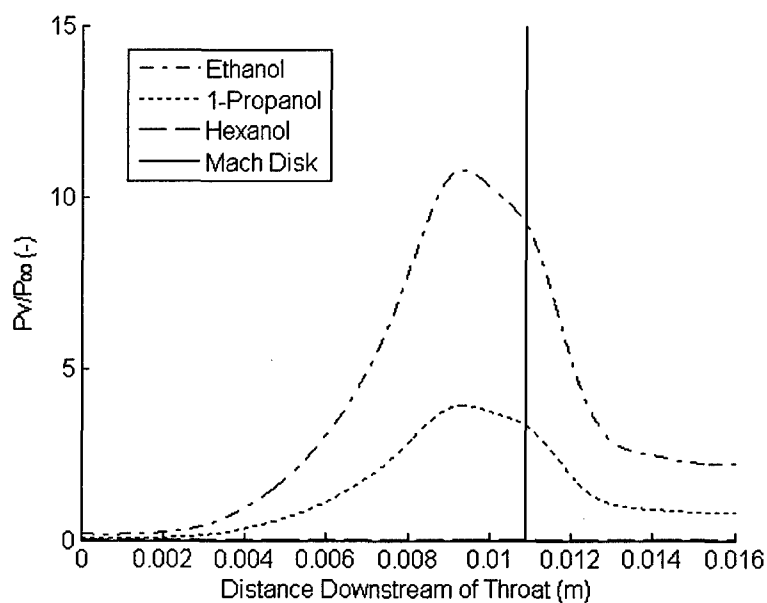


Figure 4.6 Degree of Superheat Based on Pressure for Three Test Fluids

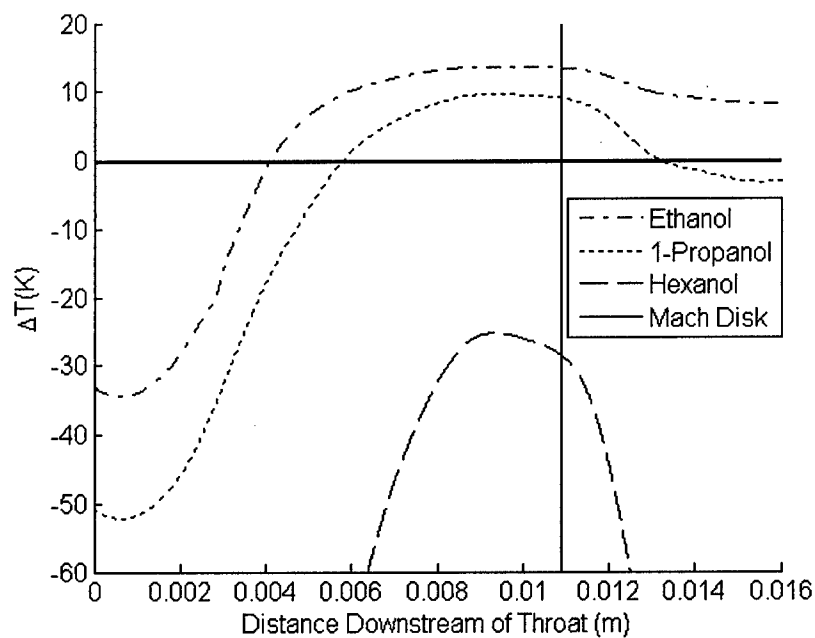


Figure 4.7a Degree of Superheat Based on Temperature for Three Test Fluids

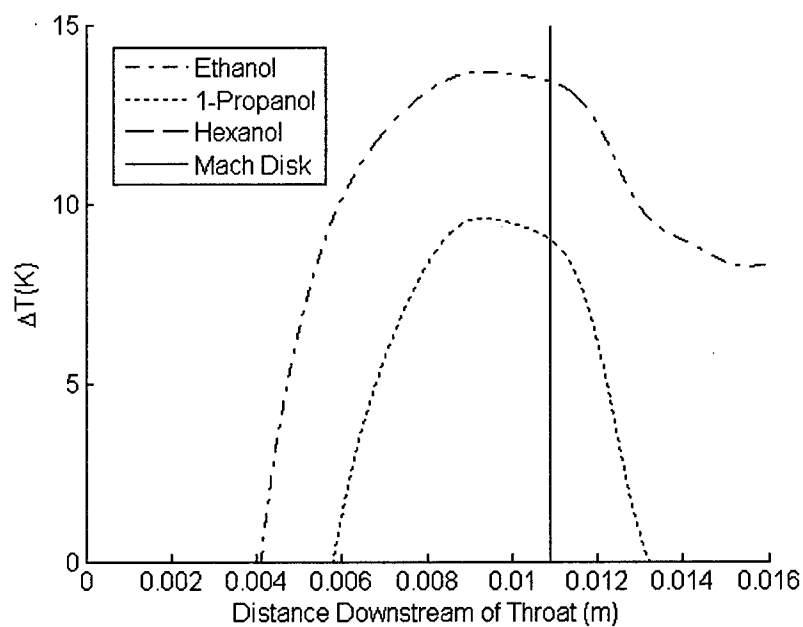


Figure 4.7b Degree of Superheat Based on Temperature for Three Test Fluids

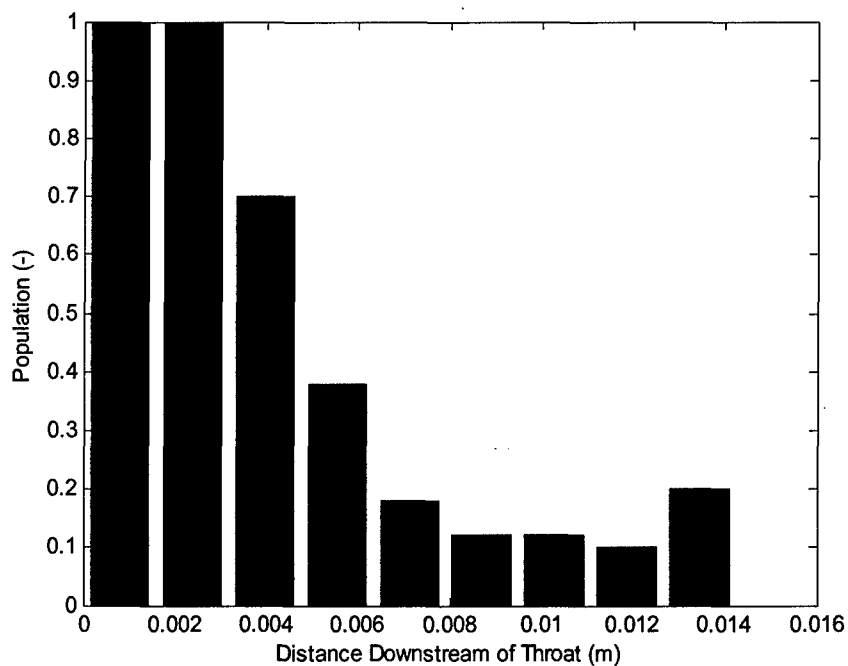


Figure 4.8 Normalized Ethanol Droplet Population Downstream of Throat

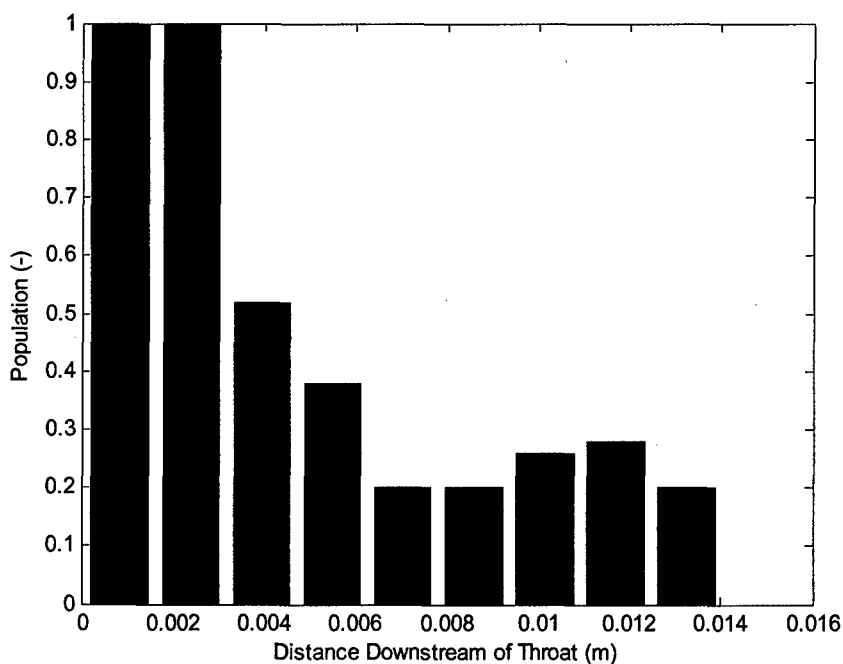


Figure 4.9 Normalized 1-Propanol Droplet Population Downstream of Throat

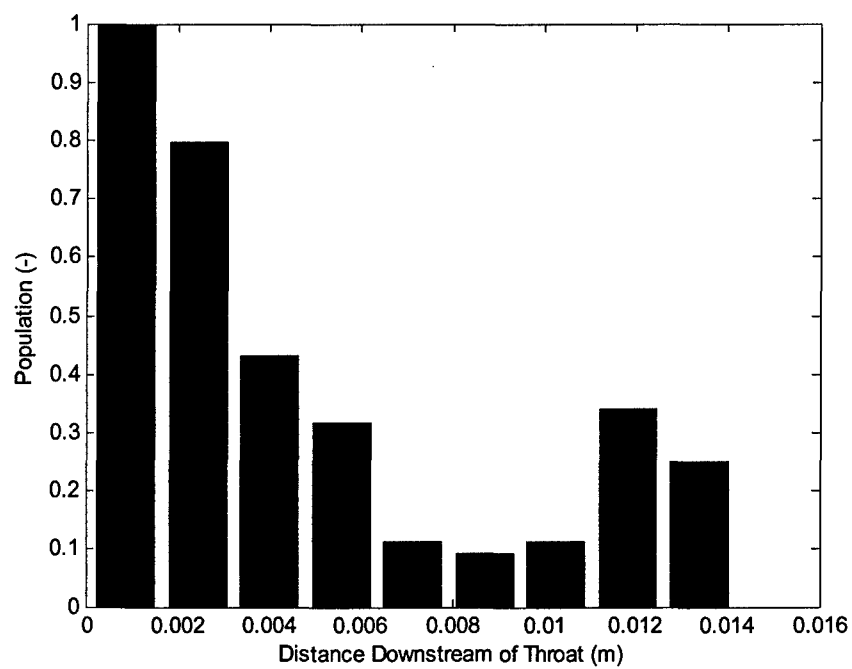


Figure 4.10 Normalized Hexanol Droplet Population Downstream of Throat

DISCUSSION

The measured absolute droplet velocity was used to determine relative velocity and Mach number:

$$M_r = \frac{v_\infty - v_d}{a_\infty}.$$

The local flow conditions (air velocity and speed of sound) were determined from the pitot probe measurements described earlier.

Of particular interest in these studies is the acceleration of the droplets subject to the known relative Mach numbers. Figures 5.1, 5.2, and 5.3 show the airflow Mach number, the droplet Mach number, the relative Mach number and the predicted solid sphere relative Mach number for ethanol, 1-propanol, and hexanol droplets, respectively. In all cases, the droplets appear to accelerate initially as predicted by the solid sphere model up to a downstream distance of about $x=0.002$ m, where the relative Mach number for the ethanol droplets deviates from the model. Both the 1-propanol and the hexanol follow the model further to a distance of approximately $x=0.0025$ m downstream of the throat. Also, the ethanol droplets reach the lowest absolute Mach number and highest Mach number relative to the flow, $M=0.45$ and $Mr=3.5$ respectively.

Hexanol droplets had the highest absolute Mach number and lowest relative Mach number, $M=0.5$ and $Mr=3.4$ respectively. The 1-propanol velocities were between the values for the other two fluids. Beyond the point at which the experimental results deviate from the hard sphere mode predictions, the droplets experience a lower drag force than predicted by the solid sphere model, which causes their acceleration to decrease, and leads to much lower absolute Mach numbers, despite the fact that the relative Mach number is rapidly increasing. It should be noted that the information provided in Figs. 5.1-5.3 is not valid downstream of the Mach disk, because of abrupt changes in the local static conditions caused by the normal shock.

It is known that droplets under these flow conditions experience a flattening normal to the airflow as the airflow around the sides lowers the pressure, stretching the droplets.¹¹ However, this increase in frontal area would be expected to increase the drag force. It is theorized that other dissipative effects are present through the mass loss of the droplets. This seems somewhat counterintuitive, as Newton's second law predicts that for a given force, a loss in mass should produce a higher acceleration. As the droplets disrupt, through evaporation

and aerodynamic breakup, it is speculated that the mass leaving the surface of the drops locally increases the mass of the airflow passing by the droplets. As momentum is conserved, the increase in mass requires that the velocity of the air decrease. The decrease in air velocity may result in a lower drag force on the bulk of the droplet accelerating it in the direction of flow. It is also theorized that droplet fragments and vapor shed primarily from the sides and leeward surface of the drop increase the momentum of the flow just downstream of the bulk of the droplet. This may create an effective thrust that partially offsets the droplet drag. Whatever the cause for the observed decrease in acceleration, it is clear from Figs. 5.1-5.3 that the acceleration is substantially less for the actual liquid drops than is predicted by the solid sphere model. This illustrates the point that the deformation and disruption of the droplets play a very significant role in the acceleration of the droplets subject to supersonic relative Mach numbers.

Relative Mach numbers were used to calculate static pressure rise across the detached bow shock expected due to the supersonic relative Mach numbers of the droplets. Figures 5.4-5.6 show the calculated normalized static

pressure before and after the bow shock with downstream distance for ethanol, 1-propanol, and hexanol droplets, respectively. The results shown in Figs. 5.4-5.6 are not valid downstream of the Mach disk.

From these pressures, the degree of superheat was calculated downstream of the normal shock. The pressure based degree of superheat is shown in Fig. 5.7, with the reference static pressure being that calculated behind the normal bow shock expected to reside on the windward side of the droplets. Figure 5.7 shows a much lower degree of superheat than Fig. 4.6 due to the static pressure rise across the bow shock upstream of the droplets. In fact, based on the static condition behind the bow shock, none of the droplet fluids are superheated at all. The trends in Fig. 5.7 are qualitatively similar to those in Fig 4.6. Figure 5.8 shows the temperature difference between the droplet at injection and the vapor pressure corresponding to the static pressure downstream of the bow shock. The saturation temperatures at the pressures downstream of the bow shock in Fig. 5.8 were determined using thermodynamic data for the three test fluids.^{35,36} Figure 5.8 can be compared to Figs. 4.7a and 4.7b (However, in Fig. 5.8 positive degrees of superheat were not achieved due to

saturation temperature at the higher pressure downstream of the bow shock being higher than the injection temperature of the droplets). It should be noted that the degree of superheat presented in Figs. 5.7 and 5.8 are for the conditions on the centerline of the windward surface of the droplets. As the airflow accelerates around the shoulders of the droplets, the static pressure decreases and the degree of superheat will move toward the levels based on freestream conditions presented in Figs. 4.6-4.7b.

Figure 5.9 shows the relative Mach numbers of the three fluid droplets plotted together along with the solid sphere model relative Mach number. In this figure, information downstream of the Mach disk is not valid because of the change in static temperature associated with the normal shock. Interestingly, droplets of the three fluids accelerate in a similar manner, all diverging from the model between 0.002 m and 0.0025 m downstream of the throat. Figure 5.9 suggests that there may be a small influence of the degree of superheat on the acceleration of these droplets. The ethanol droplets initially accelerate faster than those of 1-propanol, and hexanol respectively, (leading to a lower relative Mach number) but the ethanol droplets reach a lower absolute Mach number (i.e., a higher

relative Mach number). The three fluids were chosen to have similar properties, except for the vapor pressure, to allow for comparison between a liquid with a high degree of superheat, a moderate degree of superheat, and a liquid that would not experience superheating. While there may be some unanticipated aerodynamic breakup of the hexanol droplets, the data for hexanol and 1-propanol follow the solid sphere model somewhat better than that of the ethanol. This suggests that the difficulty in obtaining hexanol images did not preclude obtaining satisfactory droplet velocity measurements, as it is confirmed by the 1-propanol data. Additionally, the degree of superheat has an effect on the drag experienced by droplets in compressible flow.

The Weber numbers of the three fluids and the solid sphere model are plotted against the downstream distance in Fig. 5.10. In this figure, it is shown that the Weber numbers, based on initial droplet diameter and surface tension, decrease from ethanol droplets to hexanol droplets. The Weber number in all cases exceeds that predicted for the rigid sphere model. These Weber numbers suggest droplet breakup should be due to stripping or possibly catastrophic breakup as discussed earlier.

Information presented in Fig. 5.10 is not valid downstream of the Mach disk because of the instantaneous change in airflow and relative droplet velocities caused by the normal shock.

The droplet Reynolds number is plotted in Fig. 5.11 against downstream distance, again for all three test fluids and the solid sphere model. The Reynolds numbers calculated with initial droplet diameter, free stream density and viscosity, for the three fluids are very similar throughout the test section, but they differ significantly from the solid sphere model. The Reynolds numbers for the different fluids follow the same trends as the Weber number because of their dependence on relative velocity. Similarly, information downstream of the Mach disk is inaccurate due to the instantaneous change in airflow and relative droplet velocities across the normal shock.

Both the Weber Number and Reynolds number are expected to play an important role in the disruption of liquid droplets in supersonic airflow.^{11,12-30} Based on the common deviation from the solid sphere model, it is evident that there are strong aerodynamic forces influencing the deformation breakup of these droplets. Between the three

fluids, relatively smaller differences are apparent due to the degree of superheat. Higher levels of superheat cause the droplets to atomize earlier, initially accelerate faster, but ultimately reach a lower maximum velocity compared to liquids that are not superheated. The effects of superheat on drag are present, but appear to be modest in comparison to aerodynamic factors.

It is shown that the solid sphere model initially agrees with experimental results, but the liquid drops undergo changes to cause them to accelerate much slower than would be predicted from the model. In the development of a scramjet engine, this might be an encouraging finding. A slower droplet velocity before vaporization might imply a shorter combustor section while still providing ample residence time to accommodate the autoignition delay associated with the use of hydrocarbon fuel.

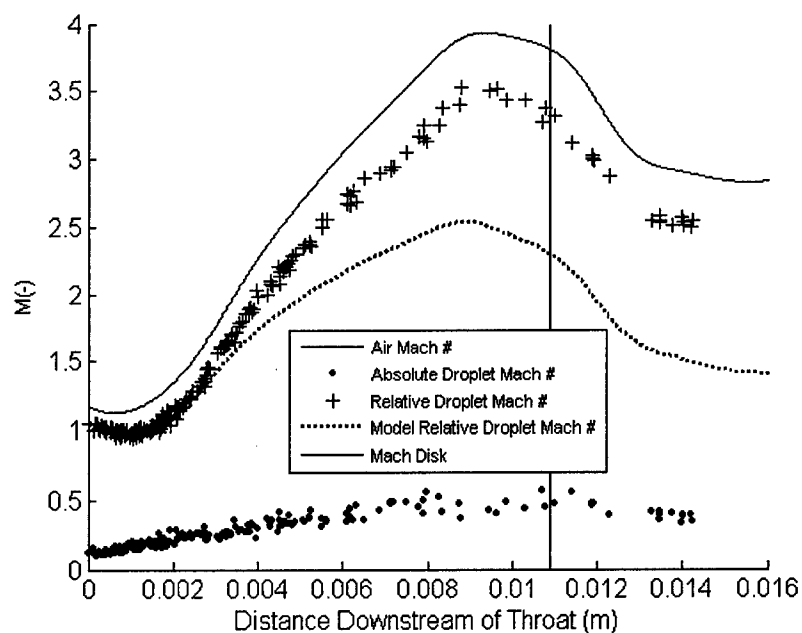


Figure 5.1 Evolution of Ethanol Droplet Absolute Mach Number, Relative Mach Number, Airflow Mach Number and Solid Sphere Mach Number With Distance Downstream of Throat

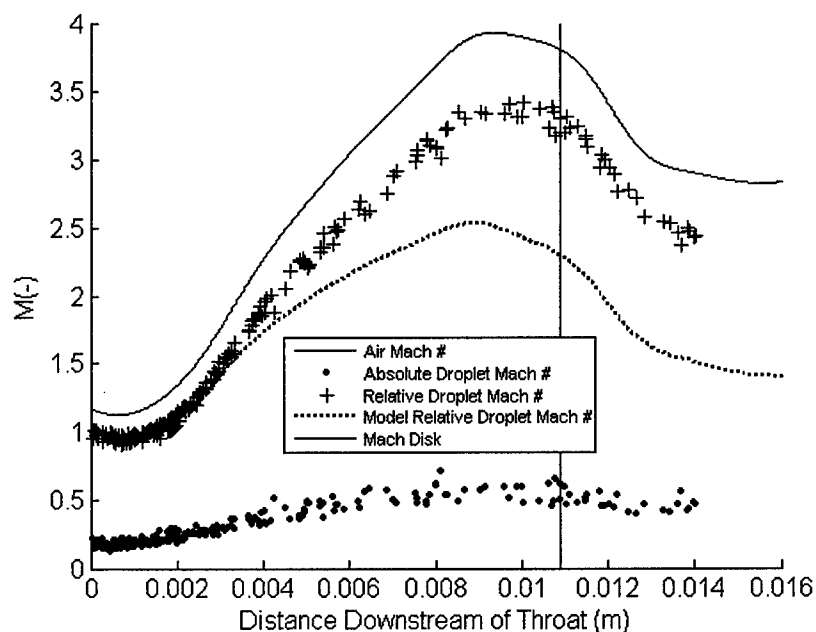


Figure 5.2 Evolution of 1-Propanol Droplet Absolute Mach Number, Relative Mach Number, Airflow Mach Number and Solid Sphere Mach Number With Distance Downstream of Throat

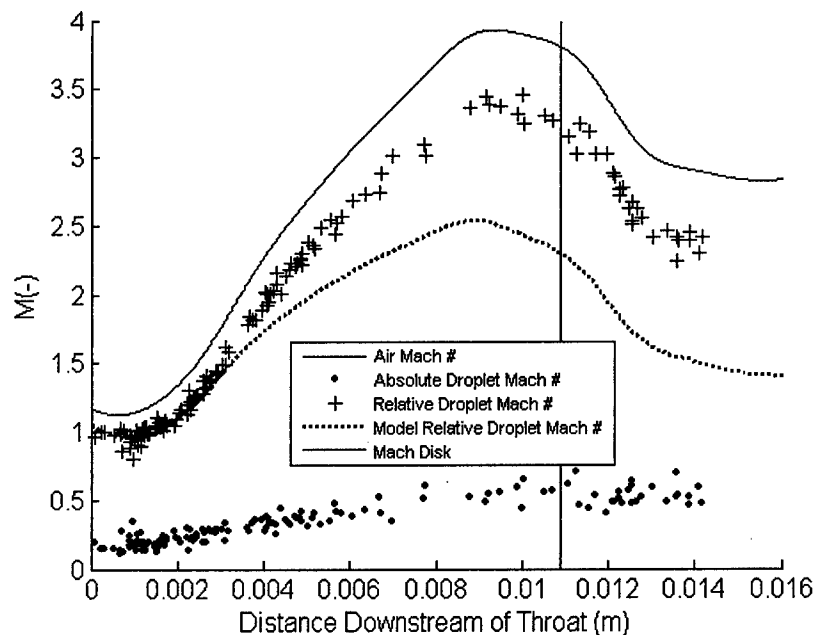


Figure 5.3 Evolution of Hexanol Droplet Absolute Mach Number, Relative Mach Number, Airflow Mach Number and Solid Sphere Mach Number With Distance Downstream of Throat

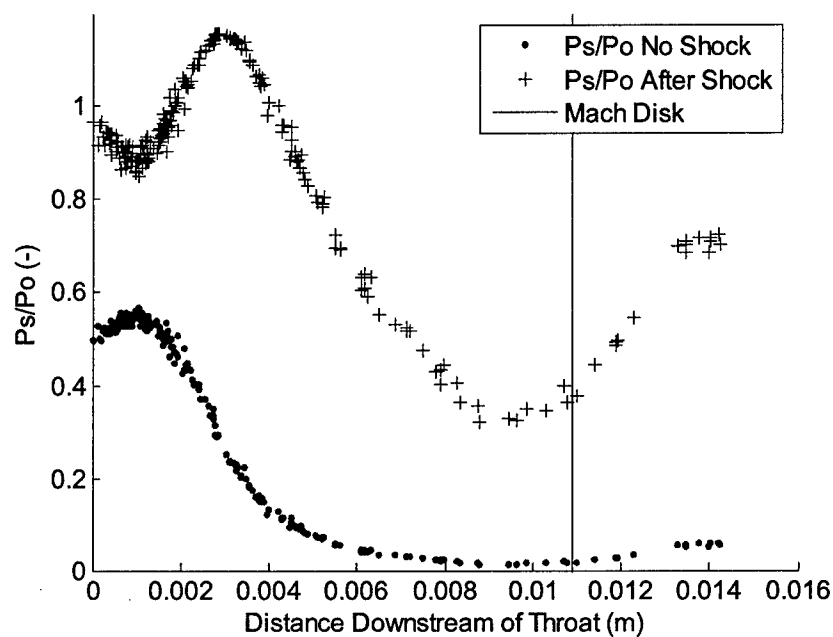


Figure 5.4 Normalized Static Pressure Without and After Detached Bow Shock for Ethanol Droplets

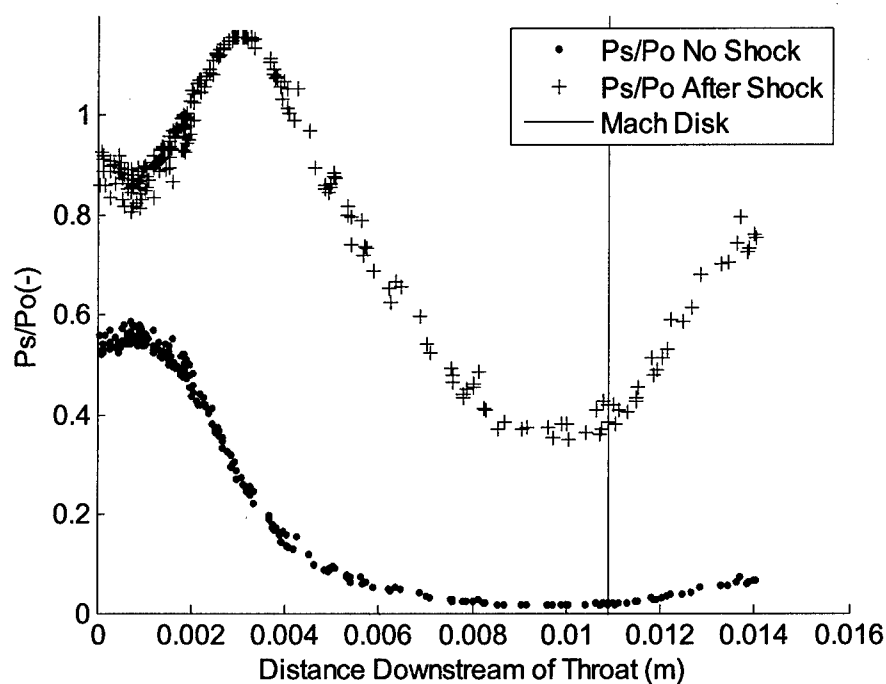


Figure 5.5 Normalized Static Pressure Without and After Detached Bow Shock for 1-Propanol Droplets

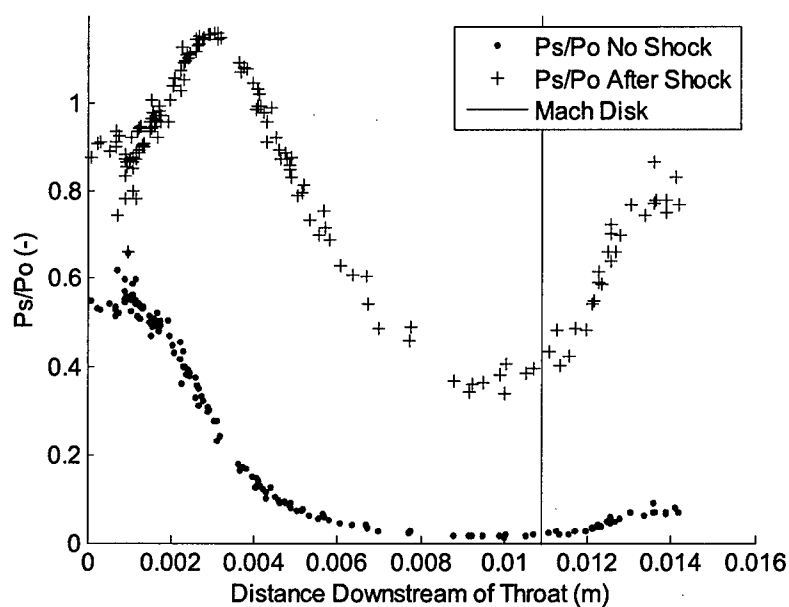


Figure 5.6 Normalized Static Pressure Without and After Detached Bow Shock for Hexanol Droplets

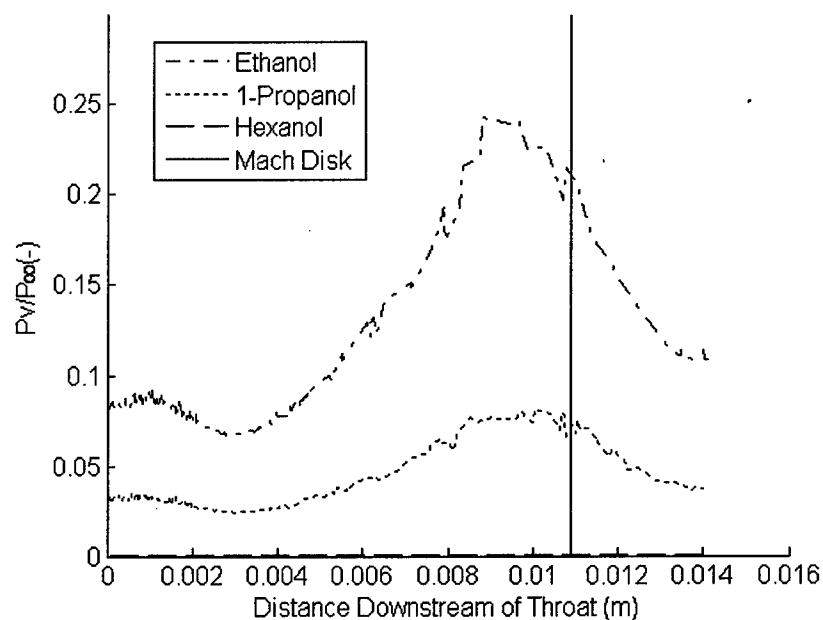


Figure 5.7 Degree of Superheat Based on Static Pressure Behind the Normal Shock for Three Test Fluids

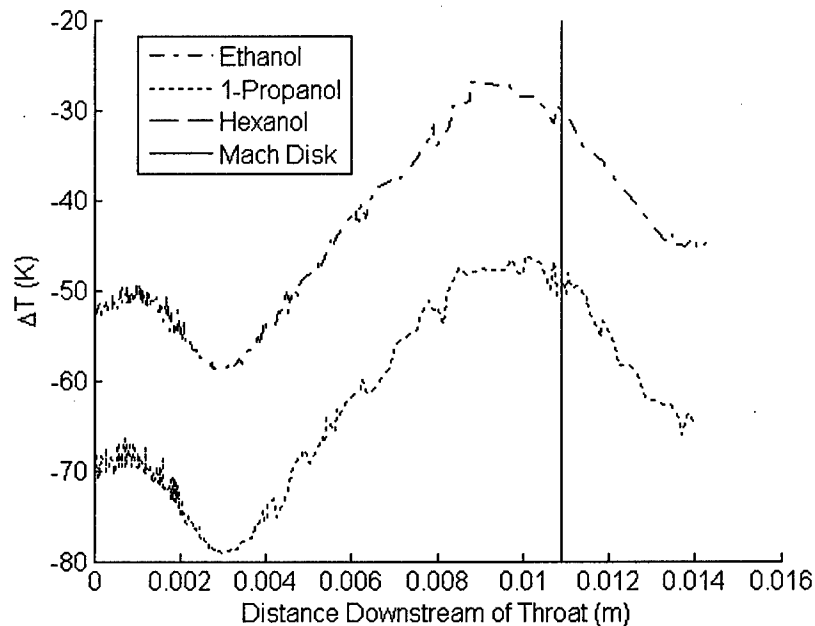


Figure 5.8 Degree of Superheat Based on Static Temperature Behind the Normal Shock For Three Test Fluids

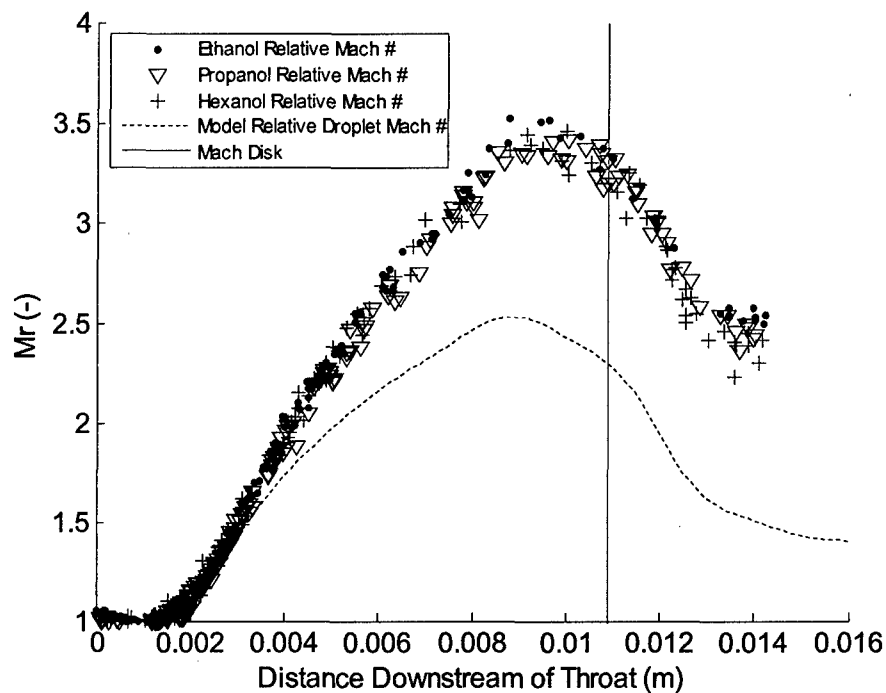


Figure 5.9 Relative Mach Numbers of Ethanol, 1-Propanol, Hexanol, and Solid Sphere Relative Mach Number vs. Distance Downstream of Throat

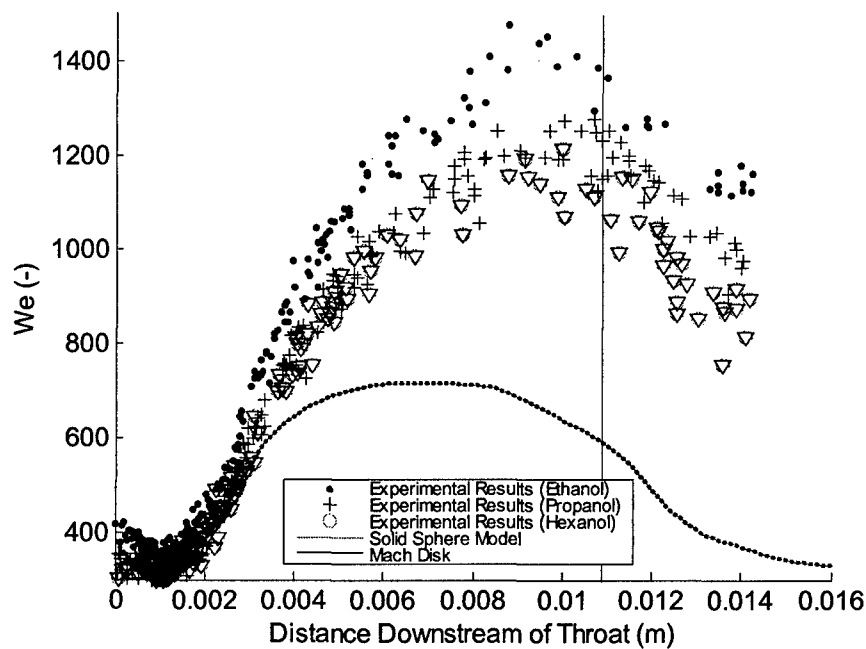


Figure 5.10 Weber Number vs. Downstream Distance

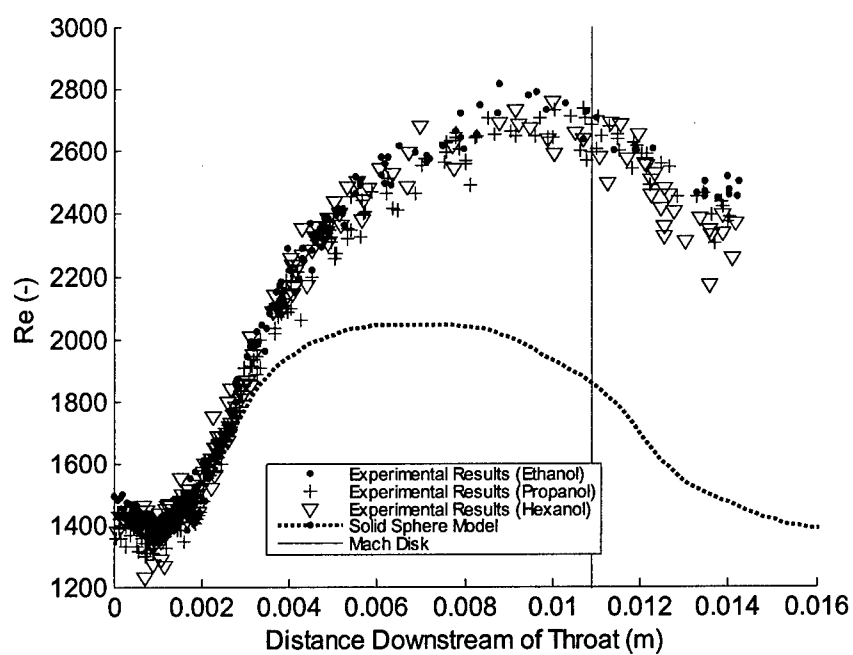


Figure 5.11 Reynolds Number vs. Downstream Distance

SUMMARY AND CONCLUSIONS

The velocities of droplets consisting of three liquid hydrocarbon fuel simulants were measured in a supersonic airflow by injecting droplets into a freely expanding jet in a draw-down supersonic wind tunnel, and imaging the droplets using a double-pulsed laser imaging technique. The goal was to compare the velocities, accelerations, relative Mach numbers, distance to disruption, and population histograms of the droplets between the liquids and with a solid sphere model of the same diameter in an airflow of known properties. The three chosen fluids, ethanol, 1-propanol and hexanol, have similar densities, and surface tensions. They vary slightly in viscosity, but have significantly different vapor pressures. The latter parameter is the primary difference between the droplets, and allows for superheating of droplets as the pressure in the test section drops below the vapor pressure for ethanol and 1-propanol.

The results suggest that droplets of all three fluids accelerate similarly, and reach similar maximum velocities which are significantly lower than predicted by the solid sphere model. The significant variation in vapor pressures represented by these three fluids does not seem to play a

major role in the accelerations or maximum velocities of the droplets. This suggests that the degree of superheat does not influence the acceleration of the droplets significantly. When compared to a solid sphere model, the measured velocities are significantly different. This disparity is likely due to deformation and disruption of the liquid droplets.

The level of superheat based on freestream static conditions was highest for the ethanol droplets, and moderate for the 1-propanol droplets. The hexanol droplets did not reach a superheated condition. However based on the static conditions just downstream of the bow shock, none of the droplets of the three liquids experienced superheating. This suggests that the effect of superheating in enhancing the disruption and vaporization primarily occurs on the flanks of the droplets rather than towards the upstream surface.

Results of this experiment show that liquid hydrocarbon droplets injected into supersonic airflow experience strong aerodynamic forces that subsequently have a significant impact on their vaporization. Additionally, they only reach velocities dramatically lower than predicted by drag data for solid spheres. These results

offer promise in future studies of supersonic droplets and in application to the design of liquid hydrocarbon fueled scramjet engines.

FUTURE WORK

Future studies should focus on better determining the role of important parameters in the breakup of superheated droplets and build a more accurate drag model for droplets in supersonic airflow. In addition to the Weber and Ohnesorge numbers, known important parameters include the mass loss and changes in shape. However, to be able to model these characteristics, it will be necessary to understand in more detail how the droplets breakup. From a time history of droplet breakup rates of mass loss and shape change can be determined.

Improved, detailed images of the disruption sequence, using back-illuminated direct photography would help bring understanding to the scientific community about droplet breakup in "steady" compressible flow, which has not been extensively studied. Further examination of droplet superheat may also offer insight into the characteristics of breakup. These tests could involve testing a fluid with similar density, surface tension, and viscosity to ethanol with a vapor pressure between that of ethanol and methanol, to gain a slightly higher degree of superheat than explored in this study. The breakup mode of the droplets may play an important role in defining a new drag model. The Weber,

Reynolds, and Ohnesorge numbers from this study have been included as they are important in describing droplet breakup.

Beyond defining the acceleration, velocity, and time at breakup, characteristics of the resulting vapor are also of interest. This could be accomplished through planar laser induced fluorescence (PLIF). Using an appropriate wavelength of light, test fluids doped with a small amount of a fluorescing substance, such as acetone, could be photographed to better understand the behavior of the resulting vapor. This may offer more insight into the mechanisms for breakup present in the current test fluids and differences in their response to supersonic airflow.

ENDNOTES

- ¹Curran, Edward T., "Scramjet Engines: The First Forty Years," *Journal of Propulsion and Power*, Vol. 17, No. 6, November-December, pp. 1138-1148.
- ²Townend, L.H., "Domain of the Scramjet," *Journal of Propulsion and Power*, Vol. 17, No. 6, November-December 2001, pp. 1205-1213.
- ³Waltrup, Paul J., "Upper Bounds on the Flight Speed of Hydrocarbon-Fueled Scramjet-Powered Vehicles," *Journal of Propulsion and Power*, Vol. 17, No. 6, November-December 2001, pp. 1199-1204.
- ⁴Kay, I.W., Peschke, W.T., and Guile, R.N., "Hydrocarbon-Fueled Scramjet Combustor Investigation," *Journal of Propulsion and Power*, Vol. 8, No. 2, March-April 1992, pp. 507-512.
- ⁵Powell, O.A., Ewards, J.T., Norris, R.B., and Numbers, K.E., "Development of Hydrocarbon-Fuels Scramjet Engines: The Hypersonic Technology (HyTech) Program," *Journal of Propulsion and Power*, Vol. 17, No. 6, November-December 2001, pp. 1170-1176.
- ⁶Colket, Meredith B., and Spadaccini, Louis J., "Scramjet Fuels Autoignition Study," *Journal of Propulsion and Power*, Vol. 17, No. 2, March-April 2001, pp. 315-323.
- ⁷Sobel, D.R., and Spadaccini, L.J., "Hydrocarbon Fuel Cooling Technologies for Advanced Propulsion," *Journal of Engineering for Gas Turbines and Power*, Vol. 119, April 1997, pp. 344-351.
- ⁸Lander, H., and Nixon, A.C., "Endothermic Fuels for Hypersonic Vehicles," *J Aircraft*, Vol. 8, No. 4, 1971, pp. 200-207.
- ⁹Yanson, L.M., Phariss, M.R., and Hermanson, J.C., "Effects of Liquid Superheat on Droplet Disruption in a Supersonic Stream," 43rd AIAA Aerospace Sciences Meeting and Exhibit, AIAA, Reno, NV, 2005, No. 2005-0351.

- ¹⁰Sornek, Rafal J., Dobashi, Ritsu, and Hirano, Toshisuke, "Effect of Turbulence on Vaporization, Mixing, and Combustion of Liquid-Fuel Sprays," *Combustion and Flame*, Vol. 120, 2000, pp. 479-491.
- ¹¹Phariss, M.R., "Effects of Liquid Superheat on Droplet Disruption and Vaporization in Supersonic Conditions," Master's Thesis, University of Washington, Seattle, 2005.
- ¹²Hsiang, L.P., and Faeth, G.M., "Drop Deformation and Breakup due to Shock Wave Steady Disturbances," *International Journal of Multiphase Flow*, Vol. 21, No. 21, 1995, pp. 545-560.
- ¹³Joseph, D.D., Bellanger, J., and Beavers, G.S., "Breakup of a Liquid Drop Suddenly Exposed to a High-Speed Airstream," *International Journal of Multiphase Flow*, Vol. 25, 1999, pp. 1263-1303.
- ¹⁴Hwang, S.S., Liu, Z., and Reitz, R.D., "Breakup Mechanisms and Drag Coefficients of High-Speed Vaporizing Liquid Drops," *Atomization and Sprays*, Vol. 6, 1996, pp. 353-376.
- ¹⁵Shraiber, A.A., Podvysotky, A.M., and Dubrovsky, V.V., "Deformation and Breakup of Drops by Aerodynamic Forces," *Atomization and Sprays*, Vol. 6, 1996, pp. 667-692.
- ¹⁶Pilch, M., and Erdman, C.A., "Use of Breakup Time Data and Velocity History Data to Predict the Maximum Size of Stable Fragments for Acceleration-Induced Breakup of a Liquid Drop," *International Journal of Multiphase Flow*, Vol. 13, No. 6, 1987, pp. 741-757.
- ¹⁷Dai, Z., and Faeth, G.M., "Temporal Properties of Secondary Drop Breakup in the Multimode Breakup Regime," *International Journal of Multiphase Flow*, Vol. 27, 2001, pp. 217-236.
- ¹⁸Krzeczkowski, Stefan A., "Measurement of Liquid Droplet Disintegration Mechanisms," *International Journal of Multiphase Flow*, Vol. 6, 1980, pp. 227-239.
- ¹⁹Liu, Z., and Reitz, R.D., "An Analysis of the Distortion and Breakup Mechanisms of High Speed Liquid Drops,"

International Journal of Multiphase Flow, Vol. 23, No. 4, 1997, pp. 631-650.

²⁰Simpkins, P.G., and Bales, E.L., "Water-drop Response to Sudden Accelerations," *Journal of Fluid Mechanics*, Vol. 55, No. 4, 1972, pp. 629-639.

²¹Wierzba, A., and Takayama, K., "Experimental Investigation of the Aerodynamic Breakup of Liquid Drops," *AIAA Journal*, Vol. 26, No. 11, 1988, pp. 1329-1335.

²²Tan, M.J., and Bankoff, S.G., "On the Fragmentation of Drops," *Journal of Fluids Engineering*, Vol. 108, March 1986, pp. 109-114.

²³Hirahara, H., and Kawahashi, M., "Experimental Investigation of Viscous Effects Upon a Breakup of Droplets in High-Speed Air Flow," *Experiments in Fluids*, No. 13, 1992, pp. 423-428.

²⁴Krauss, William E., and Leadon, Bernard M., "Deformation Fragmentation of Water Drops due to Shock Wave Impact," 12th Structures, Structural Dynamics and Materials Conference, AIAA/ASME, Anaheim, CA, No. 71-392.

²⁵Ranger, A.A., and Nicholls, J.A., "Aerodynamic Shattering of Liquid Drops," *AIAA Journal*, February 1969, pp. 285-290.

²⁶Hanson, A.R., Domich, E.G., and Adams, H.S., "Shock Tube Investigation of the Breakup of Drops by Air Blasts," *The Physics of Fluids*, Vol. 6, No. 8, August 1963, pp. 1070-1080.

²⁷Williams, Forman A., "Atomization Processes and Ignition Criteria for Supersonic Combustion with Liquid Fuel Injection," *Astronautica Acta*, Vol. 15, 1970, pp. 547-557.

²⁸Helenbrook, B.T., and Edwards, C.F., "Quasi-steady Deformation and Drag of Uncontaminated Liquid Drops," *International Journal of Multiphase Flow*, Vol. 28, 2002, pp. 1631-1657.

²⁹Li, G.J., Dinh, T.N., and Theofanous, T.G., "An Experimental Study of Droplet Breakup in Supersonic Flow: The Effect of Long-Range Interactions," 42nd AIAA Aerospace

Sciences Meeting and Exhibit, AIAA, Reno, NV, 2004, No. 2004-968.

³⁰Borisov, A.A., Gel'fand, B.E., Natanzon, M.S., and Kossov, O.M., "Droplet Breakup Regimes and Criteria for their Existence," *Journal of Engineering Physics*, Vol. 40, No. 1, 1981, pp. 44-49.

³¹Theofanous, T.G., Li, G.J., and Dinh, T.N., "Aerobreakup in Rarefied Supersonic Gas Flows," *Journal of Fluids Engineering*, Vol. 126, July 2004, pp. 516-527.

¹³Frost, D.L., "Dynamics of Explosive Boiling of a Droplet," *Physics of Fluids*, Vol. 31, No. 9, 1988, pp. 2554-2561.

³²Tseng, Fan-Gang, "Micro-Droplet Generators," Ph.D. Dissertation, National Tsing Hua University, Taiwan, 2000.

³³Charters, A.C., and Thomas, R.N., "The Aerodynamic Performance of Small Spheres from Subsonic to High Supersonic Velocities," *Journal of the Aeronautical Sciences*, October 1945, pp. 468-476.

³⁴Fox, R.W., and McDonald, A.T., "External Incompressible Viscous Flow," *Introduction to Fluid Mechanics*, 5th ed., John Wiley & Sons, Inc., New York, 1998, pp. 444-450.

³⁵Nasirzadeh, Karamat, Zimin Denys, Neueder, Roland, and Kunz, Werner, "Vapor-Pressure Measurements of Liquid Solutions at Different Temperatures: Apparatus for Use over an Extended Temperature Range and Some New Data," *Journal of Chemical and Engineering Data*, Vol. 49, No. 3, 2004, pp. 607-612.

³⁶Martinez, Santiago, Garriga, Rosa, Perez, Pascual, and Gracia, Mariano, "Isothermal Vapor-Liquid Equilibrium of 1-Chlorobuane with Ethanol or 1-Hexanol at Ten Temperatures Between 278.15 K and 323.15 K," *Journal of Chemical and Engineering Data*, No. 3, 2001, pp. 535-540.

REFERENCES

- Borisov, A.A., Gel'fand, B.E., Natanzon, M.S., and Kossov, O.M., "Droplet Breakup Regimes and Criteria for their Existence," *Journal of Engineering Physics*, Vol. 40, No. 1, 1981, pp. 44-49.
- Charters, A.C., and Thomas, R.N., "The Aerodynamic Performance of Small Spheres from Subsonic to High Supersonic Velocities," *Journal of the Aeronautical Sciences*, October 1945, pp. 468-476.
- Colket, Meredith B., and Spadaccini, Louis J., "Scramjet Fuels Autoignition Study," *Journal of Propulsion and Power*, Vol. 17, No. 2, March-April 2001, pp. 315-323.
- Curran, Edward T., "Scramjet Engines: The First Forty Years," *Journal of Propulsion and Power*, Vol. 17, No. 6, November-December, pp. 1138-1148.
- Dai, Z., and Faeth, G.M., "Temporal Properties of Secondary Drop Breakup in the Multimode Breakup Regime," *International Journal of Multiphase Flow*, Vol. 27, 2001, pp. 217-236.
- Fox, R.W., and McDonald, A.T., "External Incompressible Viscous Flow," *Introduction to Fluid Mechanics*, 5th ed., John Wiley & Sons, Inc., New York, 1998, pp. 444-450.
- Frost, D.L., "Dynamics of Explosive Boiling of a Droplet," *Physics of Fluids*, Vol. 31, No. 9, 1988, pp. 2554-2561.
- Hanson, A.R., Domich, E.G., and Adams, H.S., "Shock Tube Investigation of the Breakup of Drops by Air Blasts," *The Physics of Fluids*, Vol. 6, No. 8, August 1963, pp. 1070-1080.
- Helenbrook, B.T., and Edwards, C.F., "Quasi-steady Deformation and Drag of Uncontaminated Liquid Drops," *International Journal of Multiphase Flow*, Vol. 28, 2002, pp. 1631-1657.
- Hirahara, H., and Kawahashi, M., "Experimental Investigation of Viscous Effects Upon a Breakup of Droplets

in High-Speed Air Flow," *Experiments in Fluids*, No. 13, 1992, pp. 423-428.

Hsiang, L.P., and Faeth, G.M., "Drop Deformation and Breakup due to Shock Wave Steady Disturbances," *International Journal of Multiphase Flow*, Vol. 21, No. 21, 1995, pp. 545-560.

Hwang, S.S., Liu, Z., and Reitz, R.D., "Breakup Mechanisms and Drag Coefficients of High-Speed Vaporizing Liquid Drops," *Atomization and Sprays*, Vol. 6, 1996, pp. 353-376.

Joseph, D.D., Bellanger, J., and Beavers, G.S., "Breakup of a Liquid Drop Suddenly Exposed to a High-Speed Airstream," *International Journal of Multiphase Flow*, Vol. 25, 1999, pp. 1263-1303.

Kay, I.W., Peschke, W.T., and Guile, R.N., "Hydrocarbon-Fueled Scramjet Combustor Investigation," *Journal of Propulsion and Power*, Vol. 8, No. 2, March-April 1992, pp. 507-512.

Krauss, William E., and Leadon, Bernard M., "Deformation Fragmentation of Water Drops due to Shock Wave Impact," 12th *Structures, Structural Dynamics and Materials Conference*, AIAA/ASME, Anaheim, CA, No. 71-392.

Krzeczkowski, Stefan A., "Measurement of Liquid Droplet Disintegration Mechanisms," *International Journal of Multiphase Flow*, Vol. 6, 1980, pp. 227-239.

Lander, H., and Nixon, A.C., "Endothermic Fuels for Hypersonic Vehicles," *J Aircraft*, Vol. 8, No. 4, 1971, pp. 200-207.

Li, G.J., Dinh, T.N., and Theofanous, T.G., "An Experimental Study of Droplet Breakup in Supersonic Flow: The Effect of Long-Range Interactions," 42nd *AIAA Aerospace Sciences Meeting and Exhibit*, AIAA, Reno, NV, 2004, No. 2004-968.

Liu, Z., and Reitz, R.D., "An Analysis of the Distortion and Breakup Mechanisms of High Speed Liquid Drops," *International Journal of Multiphase Flow*, Vol. 23, No. 4, 1997, pp. 631-650.

Martinez, Santiago, Garriga, Rosa, Perez, Pascual, and Gracia, Mariano, "Isothermal Vapor-Liquid Equilibrium of 1-Chlorobutane with Ethanol or 1-Hexanol at Ten Temperatures Between 278.15 K and 323.15 K," *Journal of Chemical and Engineering Data*, No. 3, 2001, pp. 535-540.

Nasirzadeh, Karamat, Zimin Denys, Neueder, Roland, and Kunz, Werner, "Vapor-Pressure Measurements of Liquid Solutions at Different Temperatures: Apparatus for Use over an Extended Temperature Range and Some New Data," *Journal of Chemical and Engineering Data*, Vol. 49, No. 3, 2004, pp. 607-612.

Powell, O.A., Ewards, J.T., Norris, R.B., and Numbers, K.E., "Development of Hydrocarbon-Fuels Scramjet Engines: The Hypersonic Technology (HyTech) Program," *Journal of Propulsion and Power*, Vol. 17, No. 6, November-December 2001, pp. 1170-1176.

Phariss, M.R., "Effects of Liquid Superheat on Droplet Disruption and Vaporization in Supersonic Conditions," Master's Thesis, University of Washington, Seattle, 2005.

Pilch, M., and Erdman, C.A., "Use of Breakup Time Data and Velocity History Data to Predict the Maximum Size of Stable Fragments for Acceleration-Induced Breakup of a Liquid Drop," *International Journal of Multiphase Flow*, Vol. 13, No. 6, 1987, pp. 741-757.

Ranger, A.A., and Nicholls, J.A., "Aerodynamic Shattering of Liquid Drops," *AIAA Journal*, February 1969, pp. 285-290.

Shraiber, A.A., Podvysotky, A.M., and Dubrovsky, V.V., "Deformation and Breakup of Drops by Aerodynamic Forces," *Atomization and Sprays*, Vol. 6, 1996, pp. 667-692.

Simpkins, P.G., and Bales, E.L., "Water-drop Response to Sudden Accelerations," *Journal of Fluid Mechanics*, Vol. 55, No. 4, 1972, pp. 629-639.

Sobel, D.R., and Spadaccini, L.J., "Hydrocarbon Fuel Cooling Technologies for Advanced Propulsion," *Journal of Engineering for Gas Turbines and Power*, Vol. 119, April 1997, pp. 344-351.

Sornek, Rafal J., Dobashi, Ritsu, and Hirano, Toshisuke, "Effect of Turbulence on Vaporization, Mixing, and Combustion of Liquid-Fuel Sprays," *Combustion and Flame*, Vol. 120, 2000, pp. 479-491.

Tan, M.J., and Bankoff, S.G., "On the Fragmentation of Drops," *Journal of Fluids Engineering*, Vol. 108, March 1986, pp. 109-114.

Theofanous, T.G., Li, G.J., and Dinh, T.N., "Aerobreakup in Rarefied Supersonic Gas Flows," *Journal of Fluids Engineering*, Vol. 126, July 2004, pp. 516-527.

Townend, L.H., "Domain of the Scramjet," *Journal of Propulsion and Power*, Vol. 17, No. 6, November-December 2001, pp. 1205-1213.

Tseng, Fan-Gang, "Micro-Droplet Generators," Ph.D. Dissertation, National Tsing Hua University, Taiwan, 2000.

Waltrup, Paul J., "Upper Bounds on the Flight Speed of Hydrocarbon-Fueled Scramjet-Powered Vehicles," *Journal of Propulsion and Power*, Vol. 17, No. 6, November-December 2001, pp. 1199-1204.

Williams, Forman A., "Atomization Processes and Ignition Criteria for Supersonic Combustion with Liquid Fuel Injection," *Astronautica Acta*, Vol. 15, 1970, pp. 547-557.

Yanson, L.M., Phariss, M.R., and Hermanson, J.C., "Effects of Liquid Superheat on Droplet Disruption in a Supersonic Stream," 43rd AIAA Aerospace Sciences Meeting and Exhibit, AIAA, Reno, NV, 2005, No. 2005-0351.

APPENDIX A: SAMPLE SPREADSHEET

x in/pxel	X CL	x m/pxel							
0.0012 626	277	3.207E- 05							
y in/pxel	.5" mark	y m/pxel							
0.0012 755	408	3.23977 E-05							
	Y Top (in)								
	0.053571								
	Y Bottom (in)								
	0.599485								
Pictur e	x	y	Velocity m/s	x Plot From CL (in)	x Plot From CL (m)	Y From Throat (in)	Y From Throat (m)	File	
4	255	92	84.234	-0.0277772	-0.000705541	0.0803565	0.002041055	2006-01-21-1	
	255	118							
18								2006-01-21-1	
	280	391	84.296	0.0044191	0.000112245	0.461731	0.011727967		
	281	417							
23								2006-01-21-1	
	279	276	93.953	0.0025252	6.41401E-05	0.31696175	0.008050828		
	279	305							
31								2006-01-21-1	
	260	88	58.875	-0.0202016	-0.000513121	0.0701525	0.001781874		
	262	106							
39								2006-01-21-1	
	299	197	106.961	0.0284085	0.000721576	0.21874825	0.005556206		
	300	230							
72								2006-01-21-1	
	280	81	55.076	0.0037878	9.62101E-05	0.06059625	0.001538891		
	280	98							
106								2006-01-21-1	
	277	50	51.836	0	0	0.020408	0.000518363		
	277	66							